行政院國家科學委員會補助專題研究計畫 ■成果報告
□期中進度報告

砷化銦自聚式量子點內點缺陷與電子量子能階之交互作用

計畫類別：■個別型計畫　□整合型計畫
計畫編號：NSC　97－2112－M－009－014－MY3
執行期間：　99 年 08 月 01 日至　100 年 10 月 31 日
執行機構及系所：國立交通大學電子物理學系(所)

計畫主持人：陳振芳
計畫參與人員：博士班研究生-兼任助理人員：謝孟謙
博士班研究生-兼任助理人員：楊政鴻
博士班研究生-兼任助理人員：王家峰
碩士班研究生-兼任助理人員：林妍君
碩士班研究生-兼任助理人員：孫茂益

成果報告類型(依經費核定清單規定繳交)：□精簡報告　■完整報告

本計畫除繳交成果報告外，另須繳交以下出國心得報告：
□赴國外出差或研習心得報告
□赴大陸地區出差或研習心得報告
■出席國際學術會議心得報告
□國際合作研究計畫國外研究報告

處理方式：除列管計畫及下列情形者外，得立即公開查詢
□涉及專利或其他智慧財產權，□一年□二年後可公開查詢

中　華　民　國　100 年 10 月 31 日

目錄

目錄 …… I

中文摘要 …… II

英文摘要 …… III

前言 …… 1

研究目的 …… 1

研究方法 …… 1

結果與討論 …… 2

參考文獻 …… 11

圖 …… 12

表 …… 29

計畫成果自評 …… 31

附錄 …… 32

中文摘要

本研究以分子束磊晶(molecular beam epitaxy, MBE)系統成長出超越臨界厚度的砷化銦(InAs)量子點(quantum dot, QD)樣品，藉由應力鬆弛的方式誘發形成雙模態量子點，並透過光性與電性量測分析來探討雙模態量子點的形成機制與其特性。我們從穿透式電子顯微鏡顯影下觀察到錯位缺陷以及光激螢光光譜中約 70 meV 的藍移現象，可知應力鬆弛過程中所產生的兩群量子點可分為：利用生成錯位差排缺陷來達到應力釋放的低能量量子點與藉由將銦原子往外擴散與與鎵原子交換而使所承受應力減輕的高能量量子點。利用分析應力鬆弛(3.06 ML)樣品的變溫光激螢光光譜(photoluminescence, PL)可以觀察到兩群量子點間的載子轉換機制。從應力鬆弛(3.06 ML)樣品中，低能量量子點隨溫度變化的 PL 積分強度可分為兩個溫度區間：(1) 當溫度上升至 110 K 左右，強度有一異常增加的現象(2) 當溫度達到 160K 時卻下降。而高能階量子點的半高寬在 110 K 時則會下降，結合兩群量子點隨溫度變化的特性並配合模擬驗證，我們可知在溫度上升的過程中，高能階量子點中的載子會透過兩群量子點間的量子井傳輸至低能階量子點中。在應力鬆弛(3.06 ML)樣品的導納頻譜量測中，我們同樣在此溫度區間(78 K~140 K)內發現載子躍遷速率有一轉折，可以證明是由載子轉移所造成。同時利用模擬的方式驗證雙模態量子點的載子躍遷機制。

關鍵詞：砷化銦量子點、應力鬆弛、雙模態、載子躍遷機制。

Abstract

In this work we study a method for controlling of the structure of the InAs quantum dots (QDs) with InGaAs capping layer fabricated by molecular beam epitaxy (MBE) deposition. When the InAs deposition exceeds of 3 ML, strain in the InAs QDs is relaxed. At the same time, the bimodal QDs start to form. The characteristics of the bimodal QDs are studied by optical and electrical measurements. The interfaces of the GaAs buffer layer and the InAs QDs contain misfit dislocations as determined from transmission electron microscopy (TEM). The photoluminescence (PL) spectra of the bimodal QDs shows an abnormal PL blueshift of 70 meV. We observe the existence of two types of QDs in the strain-relaxed QDs system: a low energy QD family whose strain is relaxed by the generation of misfit dislocations, and a high energy QD family whose strain is mainly relieved by indium outdiffusion.

The effect of interdot carrier transfer on temperature dependent PL is investigated. The integrated-PL intensity of low energy QDs shows two regimes (i) an unusual increment begins about 110 K (ii) and then drops rapidly above 160 K. The full width half maximum (FWHM) of the high energy QDs first decreases about 110 K and reaches a minimum value at about 200 K. The phenomenon can be attributed to the carrier transfer between the bimodal QDs from the high to the low energy QDs through the InGaAs quantum well. Accordingly the carrier emission time determined by G-F measurement exhibits a V-shape versus the similar temperature dependence (78 K~140 K) due to carrier transfer between bimodal QDs in 3.3 ML sample. Based on G-F data analysis, the mechanism of carrier emission in a large electric field is likely phonon-assisted tunneling when temperature increased.

Keyword: InAs quantum dots, strain-relaxed, bimodal QDs, and carrier transfer mechanism

前言

近年來，量子點因其特殊的物理性質與光電半導體方面的多元應用而受到注目。其中，針對發展量子計算的需求，有許多研究群透過成長兩層量子點的方式來得到兩群量子點來做為研究所需要的樣品結構。我們知道當量子點磊晶厚度超過一臨界值，由於應變能太大，必定會發生應力鬆弛的機制，因此我們可以利用此機制並配合一些特定的長晶條件即可誘發量子點成為雙模態的模式。這種由一群均勻度很高的量子點因應力而自我誘發形成兩群的模式在量子點的光特性或電特性上將會有明顯的改變。

研究目的

本研究著重在探討當砷化銦(InAs)量子點(quantum dots, QDs)上方覆蓋一層砷化銦鎵(InGaAs)量子井，形成 Dot-in-well (DWELL)結構時，此結構下因應力鬆弛而形成特殊雙模態量子點的機制。最初研究 DWELL 這個結構是為了減緩晶格間的不匹配，減小量子點所承受的壓縮應力(compression stress)，以成長出密度與均勻度較高的量子點並且拉長量子點的發光波長，達到光纖通訊所需的波段。因此當我們在量子點上方覆蓋一層 $In_{0.15}Ga_{0.85}As$ 應力緩衝層時，應力鬆弛所產生的點缺陷(point defects)僅分布於量子點的內部與下方，在量子點上方並無缺陷存在，同時避免了差排缺陷(threading dislocation defects)產生。所以，我們希望能進一步的探討在 DWELL 結構中，應力鬆弛導致長波長兩群量子點形成的過程，同時瞭解此應力誘發雙模態量子點之特性，並針對雙模態量子點間載子傳輸機制做一有系統的探討。

研究方法

本研究使用分子束磊晶(molecular beam epitaxy, MBE)法在 n^+-GaAs (100)基板上成長 InAs QDs。長晶溫度485 ~ 500℃、成長步驟為先在基板上成長一層0.2 μm GaAs 緩衝層(buffer layer)，之後再成長不同厚度之InAs QDs，接著再成長48 Å InGaAs QW 蓋在 QDs 上面，長完 QW 之後再以低溫(LT)成長(500 ℃)方式成長20秒的GaAs，最後再覆蓋0.2 μm GaAs 覆蓋層(capping layer)，buffer layer；此外，capping layer摻雜矽濃度為10^{17} cm^{-3}。此研究利用不同厚度之InAs QD樣品來控制結構中應力的差異，藉此產生應力誘發之雙模態InAs/ InGaAs量子點。樣品的電性量測是利用蒸鍍鋁(Al)來形成schottky contact（陽極）及銦(In)來形成ohmic contact（陰極）。電性分析儀器方面，我們使用HP4194A 阻抗/增益相位分析儀(admittance spectroscopy)分析C-V (capacitance-voltage)及C-F (capacitance-frequency)頻

譜。光激螢光光譜(photoluminescence, PL)頻譜量測則是使用532 nm的固態雷射激發樣品所測量。

結果與討論

一.雙模態量子點形成的機制

本研究主要為探討應力誘發之雙模態 InAs/ InGaAs 量子點特性。因此在本研究的初期，我們先針對雙模態量子點形成的機制加以探討，使我們能有效的控制雙模態量子點之生長，以便我們可以對其特性與傳輸機制做進一步的探討。

使用 MBE 以 S-K Mode 的模式形成 InAs 量子點結構時，因 InAs 與 GaAs 之間的晶格常數約有 7.2% 差異，當 InAs 薄膜開始成長，為了與 GaAs 的晶格常數匹配，InAs 磊晶層在水平方向承受一壓縮應力。當 InAs 厚度超過 1.7 ML 時，應力已累積至一臨界值，InAs 的成長模式會由二維往三維轉換，藉由形成零維量子點的島狀結構來達到應力釋放，如圖 1-1 (a)。而依據磊晶層厚度的不同，我們可以得到不同大小的 QDs (2.7、3.06、3.3 ML)，在 QDs 成長完畢後，以同樣的長晶溫度(~500 ℃)覆蓋上 4.8 nm 的 $In_{0.15}Ga_{0.85}As$ QW 作為應力緩衝層，由於 $In_{0.15}Ga_{0.85}As$ 的晶格常數與量子點較接近，可減緩直接成長上 GaAs 時對量子點產生的壓縮應力。而在覆蓋 $In_{0.15}Ga_{0.85}As$ QW 的過程中，因量子點在長晶方向上所承受的是一伸張應力(tensile stress)，將吸引 QW 中的銦原子往 InAs 量子點聚集，使量子點的橫向尺寸增大（量子點基底增加）[1]，如圖 1-1 (b)所示。若緊接著以同樣的溫度成長 3.2 nm 的低溫 GaAs，則其可達到穩固量子點與得到較均勻結構的功用，如圖 1-1 (c)、(d)所示。此項技術已廣泛運用於多層量子點結構的雷射元件中[2, 3]。因為 GaAs 的長晶溫度通常在高溫 600 ℃左右，在這樣高溫的條件下，原子具有足夠的動能可做運動，而磊晶層的狀態則屬於一熔融不穩定的情況，若直接在 InAs 量子點上方覆蓋高溫成長的 GaAs，將發生得銦聚集與量子點蒸發消失的問題。當 20 秒的低溫 GaAs 長晶完畢後，會中斷成長 2 分鐘，並在這段時間內將基板長晶溫度提高到 550 ℃，在這升溫的過程中，未被低溫 GaAs 層所覆蓋住的 InAs 量子點部分將與低溫 GaAs 層產生銦鎵原子間的相互擴散(In/ Ga interdiffusion)，使量子點大小均勻性大幅增加。最後覆蓋上 0.2 μm GaAs 作 capping layer。而當 InAs 磊晶厚度超過一臨界厚度約 3 ML，如圖 1-2 (a)，InAs QDs 本身已經承受著非常大壓縮應力，此時再覆蓋上 $In_{0.15}Ga_{0.85}As$ QW，如圖 1-2 (b)，晶格不匹配的因素導致某部分體積較大的 InAs QDs 處產生差排錯位缺陷(misfit dislocation defect)來釋放部份應力。之後再長上的低溫 GaAs 失去了原先穩固 InAs QDs 的益處，反而施予 InAs QDs 更大的應力，如圖 1-2 (c)，讓沒有利用產生缺陷來釋放應力的另一部份 InAs QDs 開始透過銦鎵原子交換的過程，將銦原子往應力較低的缺陷量子點聚集[4, 5]，達到應力減緩

的效果，此時的長晶溫度(500 ~ 550 ℃)也有利於銦鎵原子交換，很類似熱退火的步驟。而整個應力釋放過程將使 QDs 成為雙模態的形式如圖 1-2 (d)所示。

二.雙模態量子點特性

充分瞭解雙模態量子點(Bimodal QDs)形成的機制之後，接下來我們將探討其結構特性與光特性。首先，我們利用穿透式電子顯微鏡(transmission electron microscope, TEM)來分析雙模態量子點在奈米尺度下空間結構上所發生的變化。圖 2-1 為 2.4 ML 與 3.06 ML Bimodal QDs 的 TEM 橫切面暗場(dark-field)圖。在 TEM 暗場圖中，影像的亮暗程度與原子序的大小相對應，亮色區域代表其組成元素的原子序較高。在 2.4 ML 樣品的 TEM 圖中我們可以清楚看到大小與形貌皆相似的量子點位在量子井結構中。量子點的形狀近似於一梯形和橢圓形，此量子點的平均高度約 8.4 nm、基底寬度約 19.6 nm。在 3.06 ML 樣品中，我們可以將量子點分為兩群，一群為大小形狀與 2.4 ML 差異較小的量子點，我們先將其稱為一致性(coherent)的 QDs，而另一群量子點不管在大小或形貌上都發生了很大的改變，我們稱為非一致性(incoherent)的 QDs。藉由 TEM 量測驗證了由應力鬆弛所誘發的雙模態量子點是確實存在。將 3.06 ML 樣品中的 coherent QDs 與 incoherent QDs 大小分別做統計，coherent QDs 的平均高度約 7.7 nm、基底寬度 26 nm，而 incoherent QDs 的平均高度約 16.1 nm、基底寬度 36.7 nm。2.4 ML 與 3.06 ML 樣品的量子點基底寬度、高度統計圖如圖 2-2 所示。將 coherent QDs 與 2.4ML 樣品的 QDs 作進一步比較，兩者在高度上無明顯變化，但 coherent QDs 的平均基底寬度增加了近 7 nm，這代表在 bimodal QDs 形成的過程中，存在着銦鎵原子間的交換(In/ Ga interdiffusion)，量子點中的銦原子會藉此過程由量子點往外擴散。在熱退火的研究中也可以發現因為 In/ Ga interdiffusion 增加而使量子點基底增寬的現象[5]。

將 3.06 ML 樣品中的 coherent QDs 和 incoherent QDs 分別做高階析度的 TEM 分析，並藉由將傅立葉轉換(fourier transform)的圖形與原圖相對應後可以清楚分辨出差排錯位缺陷與其存在的位置，如圖 2-3 所示，而圖中以圓圈圈起的部分即代表著一條 misfit dislocation defect。我們可以發現在 coherent QDs 中存在的缺陷大多分佈在量子點周圍且數目並不多，反之 incoherent QDs 內部則存在著大量的缺陷。因此驗證了我們所提出的模型：當量子點厚度超過一臨界值，某一部分體積稍大的量子點會先藉由產生 misfit dislocations defect 達到應力釋放，故在 TEM 中可觀察到缺陷的存在。而另一部份的量子點則將量子點內部的銦原子藉由銦鎵原子交換的過程將其往應力較低的地方做擴散，而系統中應力較低的位置就是缺陷產生的區域。因此在 TEM 中我們可以觀察到體積較大、形貌較特殊的 incoherent QDs。故我們再將 coherent QDs 稱為 In-outdiffusion QDs，incoherent QDs 稱為 In-cluster QDs。

在光特性方面，圖 2-4 為低溫 50 K 時固定激發能量 10mW 下不同厚度量子點的 PL 圖，我們可以發

現隨著量子點的磊晶厚度增加，其發光位置逐漸往長波長方向移動，有明顯的紅移(redshift)現象。但當量子點的磊晶超過臨界值約 3 ML 時，DWELL 量子點結構發生應力鬆弛而使厚度 3.06 ML 與 3.3 ML 樣品的 PL 光譜圖中，可以觀察到一異常的藍移(blueshift)效應[6]，因為一般對於量子點應力鬆弛的認知在於當量子點的應力減小、砷化銦量子點的能隙回復至較接近塊材能隙的大小，使其能隙值減小，對應發光的峰值將會發生紅移的情況。而在室溫 PL 圖中，圖 2-5，針對 2.7 ML、3.06 ML、3.3 ML 三片樣品做比較，除了藍移的現象外，發光 peak 由原先的 2 尖峰(peak)轉變為 3 尖峰，發光強度亦大幅減弱。接著我們比較 2.7 ML、3.06 ML、3.3 ML 三片樣品在室溫下的變功率 PL 光譜，如圖 2-6 (a)、(b)、(c)，圖 2-6 (a)中 2.7 ML 樣品針對主要發光 peak (1320 nm)作歸一化，可以發現隨著入射的激發 power 增加，額外 2 個 peak 明顯增大。當激發功率大於 50 mW 時，發光位置在 1215 nm 的 peak 強度開始大於主 peak，持續將激發功率增強至 100 mW，波長 1140 nm 的位置出現第 3 個 peak。因此我們可以確定這三個發光峰值屬於同一群量子點的基態、第一激發態(first excited state)、第二激發態(second excited state)訊號。以同樣的方式將 3.06 ML 樣品中強度最大的主 peak (1235 nm)作歸一化，隨著激發功率增加，長波長 1300 nm peak 強度減弱，而短波長 1175 nm 的 peak 卻增強，如圖 2-6 (b) 所示，可以推測這兩個發光峰值是由兩群量子點所貢獻。相似的實驗結果同樣可以在 3.3 ML 樣品中被觀察到，如圖 2-6 (c)。

因此，將 PL 中觀察到的現象與 TEM 的分析結果相互驗證可得知：在應力鬆弛過程中所產生的錯位缺陷對於樣品來說為非輻射復合中心，使 3.06 ML 與 3.3 ML 樣品的發光強度減弱。而藍移的效應則是 In/Ga interdiffusion 效應所引起；當量子點中的銦原子往缺陷的方向擴散，周圍的鎵原子隨之進入量子點內，使量子點中的銦含量減小，由原先的 InAs QDs 轉變為 InGaAs QDs，發光波長發生藍移。將不同厚度的量子點樣品中 In-outdiffusion QDs 基態訊號隨之發光能量隨溫度的變化做圖，如圖 2-7 所示，並由圖中可發現，發光峰值的放射能量隨著溫度上升逐漸下降。依據 Varshni's rule，材料能隙隨溫度的變化可藉 Varshni's fitting 做實驗數據擬合：

$$E_g(T) = E_g(0) - \frac{\alpha T^2}{T + \beta} \quad (1)$$

α、β 為材料參數，$E_g(0)$為絕對溫度 0 K 時塊材(bulk)材料的發光能隙(bandgap, E_g)，T 為絕對溫度。在此我們假設：InAs QDs 發光峰值與 InAs bulk 能隙隨溫度變化型態相似，因此可以將 Varshni's rule 的概念套用在我們的量子點樣品中，可得知當量子點樣品的組成成分不同時，α、β 的擬合參數有所不同，量子點的發光峰值隨溫度變化之斜率亦將發生改變。圖 2-7 中有 2.4 ML、2.7 ML 樣品量子點基態訊號與 3.06 ML、3.3 ML 樣品雙模態量子點中主 peak 訊號共四片樣品的發光能量隨溫度變化之曲線，圖中

虛線為 2.7 ML 樣品的實驗數據，可以發現與 2.4 ML 樣品的實驗曲線幾乎是完全重合。但對 3.06 和 3.3 ML 兩片樣品而言，其放射能量隨溫度的變化斜率與 2.7 ML 有明顯差異，以 3.06 ML 樣品為例：低溫 50 K 時相對 2.7 ML 樣品的峰值藍移量為 67 meV，室溫 300 K 時則降為 51 meV。由此推估實驗中 3.06 ML 與 3.3 ML 發光峰值所對應的量子點在組成成份上必與 2.7 ML 和 2.4 ML 樣品的量子點有所差異。因此我們推測在應力鬆弛雙模態量子點形成的過程中藍移效應確實是因為某一群量子點中的銦原子往缺陷的方向擴散，使其量子點中的銦含量減小，由原先的 InAs QDs 轉變為 InGaAs QDs 所造成。因此，由上述的實驗結果，可以確認：在應力鬆弛誘發的雙模態量子點 PL 光譜中，1300 nm 長波長的發光峰值代表的是 In-cluster 量子點的訊號，而短波長的兩個波峰訊號則由 In-outdiffusion 量子點的基態與激發態所貢獻。

我們進一步利用 DLTS 來分析應力鬆弛之樣品(3.06 ML 與 3.3 ML)，將樣品的量測偏壓與速率窗(rate window)固定，增加填充偏壓時間(filling pulse time)，在 3.06 ML 與 3.3 ML 樣品中量測到的缺陷訊號皆會達到飽和，如圖 2-8(a)、(b)所示，由此可確定樣品中的差排錯位缺陷屬於一種點缺陷(point defect)，證實 DWELL 結構確實有效避免了線差排缺陷(threading dislocation)的產生。在實驗中，3.3 ML 樣品所量測到的飽和值 ΔC 大了 3.06 ML 樣品約一個數量級，可知當量子點磊晶厚度超過臨界值後，持續將磊晶厚度增加會使缺陷濃度提高。圖 2-9(a)、(b)為二片樣品在固定偏壓與 filling pulse time 下改變不同的 rate window 所得到的 DLTS 量測結果，將不同 rate window 實驗曲線所對應到的峰值溫度繪製成阿瑞尼士圖(Arrhenius plot)，如圖 2-10，可由此得到缺陷的活化能(activation energy)和捕捉截面積(capture cross section)。而 3.06 ML 及 3.3 ML 樣品不管在的活化能或捕捉截面積都非常相近，約 380 meV 和 10^{-17} cm^2，如表 1 所示。因此這兩片樣品中的缺陷應該是屬於同一種類型。目前我們推測此種缺陷為鎵空缺(Ga vacancy)與砷間隙原子(As interstitial) 復合型的 EL6 (E_C－0.35 eV)缺陷(As_i–V_{Ga} complex) 。

三. 雙模態量子點間載子傳輸機制

由雙模態量子點特性分析可得知，當量子點發生應力鬆弛時，我們將在室溫光激螢光譜中觀察到一反常的藍移，藍移量約 70 meV，並在波長 1300 nm 附近出現了一個低能階訊號。並且，在 3.06 ML 與 3.3 ML 樣品 PL 光譜中的三個峰值可分為：產生錯位缺陷並引發 In 原子聚集的量子點(In-cluster QDs)將貢獻低能階峰值訊號，而高能階峰值訊號則來自於 In 原子向外擴散的量子點(In-outdiffusion QDs)，可分為基態和第一激發態。接下來我們將進一步探討探討雙模態量子點間載子的傳輸機制。

在不同溫度下對3.06 ML樣品做PL量測，如圖3-1所示。隨著溫度上升，晶格間的鍵結減弱，使量子點能隙減小而在發光訊號上可看見明顯紅移。進一步將PL光譜圖中的三個峰值以三個高斯曲線作擬

合，擬合結果如圖3-2(a)、(b)所示。藉由這方法我們可知三個峰值的發光強度(PL intensity)、半高寬(full width at half maximum, FWHM)、發光能量位置(peak position)在溫度變化下所做的改變。將變溫的In-cluster QDs基態訊號與In-outdiffusion QDs基態訊號作比較，首先在歸一化PL積分強度上可觀察到一異常的現象，如圖3-3，低能階In-cluster QDs訊號在溫度110 K到160 K範圍內，隨著溫度上升而PL強度增強，與以往所認知的隨溫度上升而量子點侷限效應減弱使發光強度減小的熱抑制效益(thermal quenching effect)相互矛盾。配合半高寬對溫度的變化圖，如圖3-4，高能階In-outdiffusion QDs的半高寬曲線一開始隨溫度上升而下降，並在200 K時出現最小的半高寬值(~47 meV)，隨後則隨溫度上升而半高寬值增大。一般來說，由於高溫時的聲子散射(phonon scattering)效應較強，使導帶中電子與價帶中的電洞的能量分佈範圍增加，因此，量子點的半高寬值也會隨溫度上升而增加。在一些團隊的研究中[7-9]證實，當量子點系統內發生載子重新分佈或轉移的現象時，在半高寬曲線中將會觀察到隨溫度變化的V型曲線。藉由半高寬與PL積分強度的相互佐證，我們可以證明在應力釋放雙模態量子點間存在著載子傳輸的現象。而載子傳輸的機制有穿隧效應(tunneling effect)與熱激發(thermal activation)兩種可能，半高寬與積分強度訊號在溫度變化下有明顯的改變，而在TEM的量測中，高低能階量子點間的距離約20 nm，因此我們將兩群量子點之間的穿隧效應忽略，單純考慮熱激發的情況。低能階In-cluster QDs在溫度上升至110 K時積分強度有一明顯上升，推測是因為有額外的載子由外部對量子點做補充，使發光強度增強，配合In-outdiffusion高能階量子點半高寬在約110 K的溫度點開始下降，代表有足夠數量的載子因溫度上升獲得熱能而脫離量子點，使量子點發光範圍集中。半高寬與積分強度發生轉折的溫度點可相互對應，因此我們推測隨著溫度上升載子會由高能階In-outdiffusion QDs傳輸至低能階In-cluster QDs中。

針對低能階In-cluster QDs在110 K時所觀察到的發光強度異常上升現象，我們利用速率方程式模型(rate-equation model)所得到公式進行擬合，進一步驗證我們所作的推測，並期望能找出載子傳輸的路徑，利用公式3-1[10,11]的擬合結果如圖3-5所示。

$$I(T)=\left\{1+\frac{K_o}{1+A\exp\left(-E_{A1}/k_BT\right)}\cdot\left[1+K_1\exp\left(-E_{A2}/k_BT\right)\right]\right\}^{-1} \qquad (2)$$

其中 $I(T)$代表隨溫度變化下低能階量子點的 PL 發光積分強度、k_B是波茲曼常數(Boltzmann’s constant)，E_{A1}、E_{A2}為活化能，K_0、K_1、A、B 則是擬合常數，T 為絕對溫度。最佳的擬合結果：E_{A1} 值為 122 meV、E_{A2} 值為 165 meV，其餘的擬合參數 K_0、K_1、A 分別為 3320、4.5×10^5、3.04×10^4。將溫度 110 K 時的 PL 量測結果以導電帶與價電帶比 7 : 3(CB : VB = 7 : 3)的比例計算下可以得到 3.06 ML 樣品中詳細的

能帶圖，如圖 3-6 所示，導電帶中高能階 In-outdiffusion QDs 基態和量子井的能階差約 126 meV。而低能階 In-cluster QDs 與量子井的能量差為 168 meV。將公式擬合出的活化能值與由 PL 量測所得到的能帶圖相互比對，其中 E_{A1} 與高能階量子點基態至量子井的能階差相近，E_{A2} 則可與低能階量子點基態至砷化銦鎵量子井的能階差相對應。藉由公式的擬合，我們可以知道載子傳輸的發生與溫度有很大的關係，低溫時高能階 In-outdiffusion QDs 中的載子被侷限在量子點內，當溫度上升，載子獲得足夠能量克服能障，脫離量子點的侷限，利用連接二群量子點間的砷化銦鎵量子井作為路徑傳輸至低能階 In-cluster QDs 中，使低能階量子點的光激發強度上升。因低能階量子點與量子井間有著較大的的導電帶差(conduction band offset)值，其量子點局限效應較佳，溫度必須上升至約 160 K 時，載子才有足夠的能量藉由量子井逃脫，故 PL 激發強度將再度下降。並因訊號過弱，量測溫度 200 K 以上的 PL 光譜圖必須將雷射激發光源的功率增加，而為了確保每個溫度下的量測條件皆相同，我們用來擬合的實驗值將只取到 190 K。

接著，我們利用導納頻譜分析(C-F analysis)來探討雙模態量子點間載子之傳輸機制。圖 3-7 為 3.3 ML(應力鬆弛)樣品在各偏壓下得到之導納頻譜量測結果所繪製而成的阿瑞尼士圖(Arrhenius plot)，由圖中可發現 3.3 ML 樣品的載子躍遷速率大致分為兩個區域，低溫的載子躍遷速率基本上不隨溫度改變而變動，由穿隧機制主導。高溫時隨溫度上升載子躍遷速率增加，明顯受到熱激發所影響。值得注意的是當負偏壓大於 2.6 V 時，載子躍遷速率在溫度 120 K 附近有一 V 型的變化，屬於先變慢再變快的情形。根據上述的結果，此現象與兩群量子點間的載子轉移有關，在低溫 78 K 至 120 K 溫度區間內會先量測到高能階 In-outdiffusion QDs 的躍遷時間，其侷限能階與 GaAs 導帶間的能量差較小，因此載子的躍遷速率較快。而當溫度上升至 140 K 的過程中，高能階 In-outdiffusion QDs 中的載子會轉移至低能階 In-cluster QDs 中，費米能階(Fermi-level)掃到低能階量子點，這時候量測到的載子是由較深的侷限能階躍遷而出，故我們得到的載子躍遷速率將減慢。由此我們可以知道兩群量子點間的載子轉移與偏壓、溫度皆有很大的關係。

將導納頻譜分析中所得到的載子躍遷速率與溫度平方乘積取對數後對溫度倒數作關係圖，如圖 3-8，我們先針對熱激發主導載子躍遷速率的溫度區域以 3-2 式擬合，求出各偏壓下所對應的活化能值，如表 2 所示。

$$e_{th}(T) = \gamma T^2 \sigma_n \exp\left(-E_a \big/ k_B T\right) \tag{3}$$

其中 γ 為一常數，對 n-type GaAs 而言其值為 $2.28\times10^{20}\ \mathrm{cm^{-2}s^{-1}K^{-2}}$，$\sigma_n$ 為捕捉截面積、E_a 為活化能。由表 2 中可知隨著外加負偏增大，Fermi-level 往量子點底部的方向掃動，量子點中的載子受熱激發躍遷

而出時所必須克服的位能障即是由公式所擬合出的活化能。若將擬合出的活化能值與圖 3-9 中由 PL 量測所得到的能帶圖相比較，可以發現由電性量測所得到的模擬值遠小於由光性量測的結果，代表在高溫時的載子躍遷機制應該不是單純由量子點內部獲得足夠熱能後跳至 GaAs 導電帶的熱躍遷。

若同時考慮摻雜濃度與外加偏壓條件下，我們將會得到非常大的電場，以摻雜濃度 $N_D - N_A = 10^{18}$ cm^{-3}、外加偏壓 $V_a = -3$ V 為例，系統中得到的電場高達 10^8 V/m，因此我們必須將電場效應考慮進受熱激發的載子躍遷過程中。由圖 3-7 可以知道，在負偏大於－2.6 下，溫度 140 K 時載子躍遷機制處於熱激發與穿隧機制的臨界點。利用 140 K 時的高頻 C-V 量測下的電容值，如圖 3-10 所示，可計算出空乏區寬度 W、電場 E、電位 Φ，如圖 3-12 所示：.

$$C_H = \frac{\varepsilon_o \varepsilon_r A}{W} \tag{3}$$

$$E = \frac{qN_d\left(W - L_{dot}\right)}{\varepsilon_o \varepsilon_r} \tag{4}$$

$$\Phi = \frac{qN_d\left(W - L_{dot}\right)^2}{2\varepsilon_o \varepsilon_r} \tag{5}$$

其中 C_H 為高頻電容值、自由空間電容率 $\varepsilon_0 = 8.85 \times 10^{-12}$ F/m、介電常數 $\varepsilon_r = 13.1$、金屬接面面積 $A = 5.024 \times 10^{-3}$ cm^{-3}、量子點於表面的距離 $L_{dot} = 0.2$ μm，由圖 3-11 的轉縱深圖得到樣品的等效摻雜濃度 $N_d = 0.3 \times 10^{-17}$ cm^{-3}，各偏壓下計算得到的電場與電位如表 3 所示。由模擬出的電位值可與圖 3-9 中 PL 量測所得的能帶圖相互對應，可知各偏壓下 Fermi-level 所掃到的能階位置。將模擬出的電位能與由 G-F 實驗所得到的活化能值相對應，可以發現在大負偏下的活化能遠小於電位能，因此我們推測在大偏壓下，載子的躍遷機制應屬於兩段式的放射過程，載子受熱激發後由侷限能階躍遷一段能量距離至某一能階位置後，再克服位能障礙後穿隧而出。

將各偏壓下隨溫度變化的載子躍遷時間分別以公式(3)與公式(6)針對高溫區的熱躍遷與的低溫區的穿隧機制以 Mathcad 軟體進行擬合

$$e_{tun}\left(F\right) = \frac{qF}{4\sqrt{2m^* E_b}} \exp\left[-\frac{4}{3}\frac{\sqrt{2m^* {E_b}^3}}{q\hbar F}\right] \tag{6}$$

其中 F 為電場、m^*為等效質量、E_b 為穿隧能障(tunneling barrier height)，由公式 3-4 可看出當外加偏壓固定時，穿隧速率是一個與溫度無關的固定值。大小偏壓下載子躍遷時間的模擬結果如圖 3-13 (a)、(b)所示，高溫區的熱躍遷位能障 E_h 即是活化能 E_a，而以低溫區的實驗數據則可得到穿隧位能障的高度，將其統計於表 3 中。由表 3 我們可知，小偏壓下模擬得到的穿隧位能障與活化能大小極為近似，此時的 Fermi-level 掃到較淺的能階，故低溫時載子的放射機制屬於純穿隧效應，當量測溫度升高，載子獲得足夠熱能，將改以單純熱激發的方式躍遷離開侷限能階，如圖 3-13 (a)。而當外加偏壓增大，Fermi-level 掃到的能階位置較深，模擬得到的穿隧位能障 E_b 與 InGaAs QW 和 GaAs CB 能階差相近。活化能大小

則近似於侷限能階至 InGaAs QW 的能量距離。由此我們可知當溫度上升，載子會先由侷限能階躍遷至 InGaAs QW 能階後再穿隧而出，如圖 3-13 (b)所示，屬於兩段式的載子放射機制，故將活化能與穿隧位能相加總後的值近似於電位能。二段式的載子躍遷過程即屬於聲子助穿隧效應(phonon assisted tunneling)，同時考慮電場效應與聲子偶合(phonon coupling)效應，電子與聲子間的偶合作用(electron-phonon coupling)對引起熱助穿隧(thermally assisted tunneling)有很大的幫助，而載子總躍遷速率為純熱躍遷速率與純穿隧速率的總合[12]

$$\frac{1}{\tau_{total}}=\frac{1}{\tau_{th}}+\frac{1}{\tau_{tun}} \tag{7}$$

由公式 3-5 可知，對載子的兩段式躍遷而言，其載子逃脫速率會遠比單純的熱躍遷或穿隧來得快。

四. 結論

本論文利用應力鬆弛的方式使厚度3.06 ML及3.3 ML的砷化銦量子點在覆蓋一層砷化銦鎵應力緩衝層的結構下成為了雙模態量子點的模式，並透過光性與電性的分析來了解量子點在性質上的改變。當InAs QDs磊晶厚度超過一臨界值約3 ML，量子點承受著非常大的壓縮應力，後續覆蓋上$In_{0.15}Ga_{0.85}As$ QW的過程中，兩層結構間的晶格不匹配導致某部分體積較大的InAs QDs在異質接面處與量子點內部產生misfit dislocation defect來釋放部份應力。而之後在成長上的GaAs capping layer將施予InAs QDs更大的應力，讓沒有利用產生缺陷來釋放應力的另一部份InAs QDs開始透過銦鎵原子間交換的過程，將銦原子往應力較低的缺陷量子點聚集，達到應力減緩的效果，而因為不同的應力釋放方式將使量子點具有不同性質，使量子點系統成為雙模態的形式。應力鬆弛所造成的兩群量子點與2.7 ML單群量子點相比，在PL光譜中可以觀察到約70 meV的藍移、發光強度大幅下降、並在波長1300 nm的位置出現一低能階量子點訊號。由DLTS實驗可量測到在應力鬆弛過程中所產生的缺陷，而缺陷能階位置大約在砷化鎵導帶下方380 meV左右，量測結果可與TEM中在量子點底部附近與內部所觀察到的錯位缺陷相對應。因此我們更加確定雙模態量子點是由產生錯位缺陷並使銦聚集的低能階In-cluster QDs與透過銦鎵原子間交換將量子點中的銦原子往低應力缺陷區域聚集的高能階In-outdiffusion QDs所組成。

利用3.06 ML樣品的變溫PL光譜所得到的發光峰值積分強度與半高寬進行分析，在溫度110 K時可以觀察到低能階的In-cluster QDs在發光強度有一異常的上升，而同樣溫度下則對應到高能階的In-outdiffusion QDs半高寬值下降，這些特性都指向在高低能階量子點間存在著載子傳輸的現象。藉由擬合低能階量子點的積分強度，我們可以知道載子傳輸的發生是由於當溫度上升，高能階量子點中的載子獲得足夠能量並脫離量子點的侷限，利用二群量子點間的砷化銦鎵量子井作為路徑傳輸至低能階量子點中，因而使低能階量子點的光激發強度上升。

在 3.3 ML 樣品中，透過導納頻譜的量測得到定偏壓下不同溫度的載子躍遷速率，由量測結果可知在低溫時的載子躍遷速率不受溫度影響，屬於純穿隧的機制，而高溫時的載子躍遷則明顯受到熱激發所影響。在大負偏壓下，由於兩群量子點間的載子轉移效應使載子躍遷速率於溫度 120 K 附近有一 V 型的轉折變化。利用模擬驗證可以確定在大偏壓量測下，隨溫度上升過程中，載子獲得足夠能量後可由侷限能階熱躍遷至 InGaAs QW 後再穿隧而出，使載子的躍遷速率增加。

參考文獻

[1] M. V. Maximov, A. F. Tsatsul'nikov, B. V. Volovik, D. S. Sizov, Yu. M. Shernyakov, I. N. Kaiander, A. E. Zhukov,A. R. Kovsh, S. S. Mikhrin, V. M. Ustinov, and Zh. I. Alferov, R. Heitz, V. A. Shchukin, N. N. Ledentsov, and D. Bimberg, Phys. Rev. B **62**, 16671 (2000)

[2] N. N. Ledentsov, J. Böhrer, D. Bimberg, I. V. Kochnev, M. V. Maximov, P. S. Kop'ev, Zh. I. Alferov, A. O. Kosogov, S. S. Ruvimov, P. Werner, and U. Gösele, Appl. Phys. Lett. **69**, 1095 (1996).

[3] N N Ledentsov, M V Maximov, D Bimberg, T. Maka, C M Sotomayor Torres, I V Kochnev, I L Krestnikov, V M Lantratov, N A Cherkashin, Yu M Musikhin, Zh I Alferov, Semicond. Sci. Technol. **15**,604 (2000).

[4] L. J. M. Selen, L. J. van IJzendoorn, and M. J. A. de Voigt P. M. Koenraad, Phys. Rev. **B** 61, 8270 (2000).

[5] Adam Babiński, J. Jasiński, R. Bożek, A. Szepielow, and J. M. Baranowski, Appl. Phys. Lett. **79**, 2576 (2001).

[6] 陳宜屏,交通大學電子物理研究所碩士論文, "氮含量與砷化銦厚度對砷化銦/砷化鎵量子點光性影響" (2003).

[7] A. Fiore, P. Borri, W. Langbein, J. M. Hvam, U. Oesterle, R. Houdré, R. P. Stanley, and M. Ilegems, Appl. Phys. Lett. **76**, 3430 (2000).

[8] D. I. Lubyshev, P. P. González-Borrero, E. Marega, E. Petitprez, N. La Scala, and P. Basmaji, Appl. Phys. Lett. **68**, 205 (1996).

[9] S. Sanguinetti, M. HeniniM, Grassi Alessi, M. Capizzi, P. Frigeri and S. Franchi Phys. Rev. B **60**, 8276 (1999).

[10] Dan P Popescu, Peter G Eliseev, Andreas Stintz, and Kevin J Malloy, Semicond. Sci. Technol. **19**, 33 (2004).

[11] Dan P Popescu, Peter G Eliseev, Andreas Stintz, and Kevin J Malloy, Proc. SPIE 4999, 486 (2003)

[12] V. Ciulin, S. G. Carter, M. S. SherwA, Huntington, and L. A. Coldren, Phys. Rev. B **70**, 115312 (2004).

(a) QDs: 1.7ML-3ML

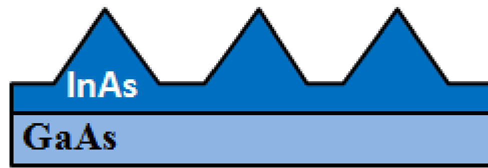

(b) $In_{0.15}Ga_{0.85}As$:4.8 nm

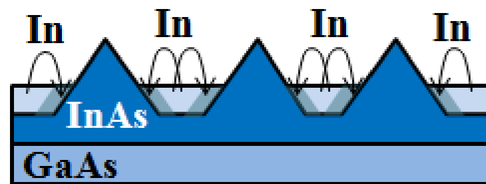

(c) LT GaAs : 3.2 nm

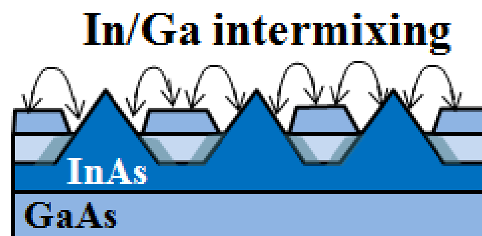

(d)

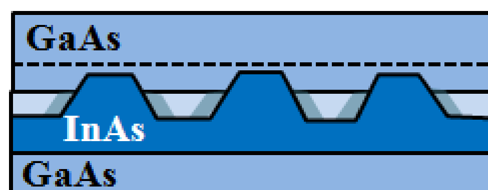

圖 1-1　厚度 3ML 以下的量子點長晶過程

(a) QDs > 3ML

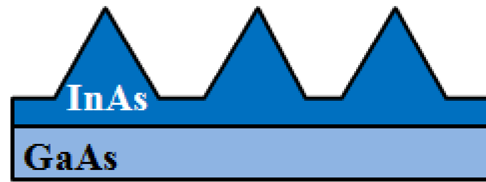

(b) $In_{0.15}Ga_{0.85}As$:4.8 nm

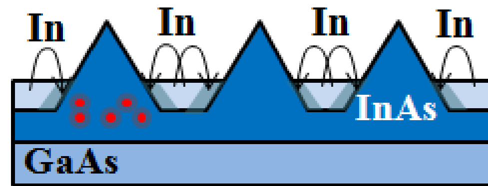

(c) LT GaAs : 3.2 nm

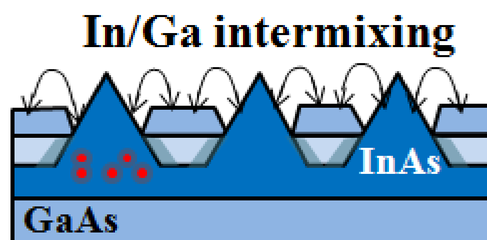

(d)

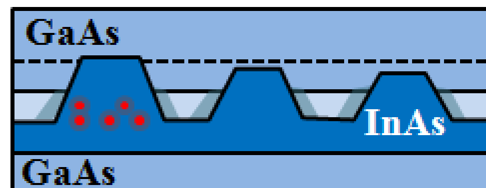

圖 1-2　厚度 3ML 以上的量子點形成雙模態模式之長晶過程

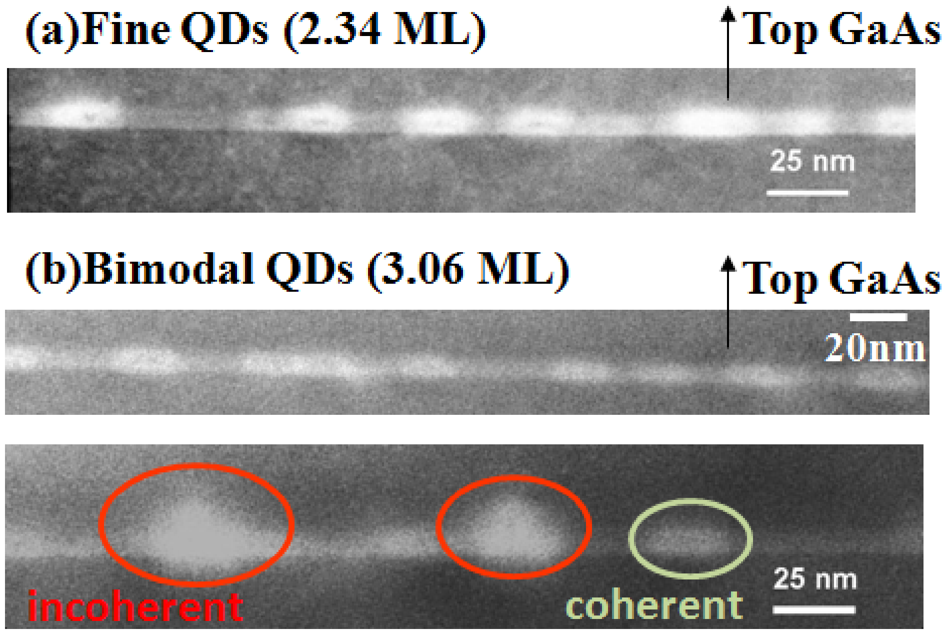

圖 2-1　(a) 2.4 ML 與(b) 3.06 ML 雙模態量子點之 TEM 比較圖

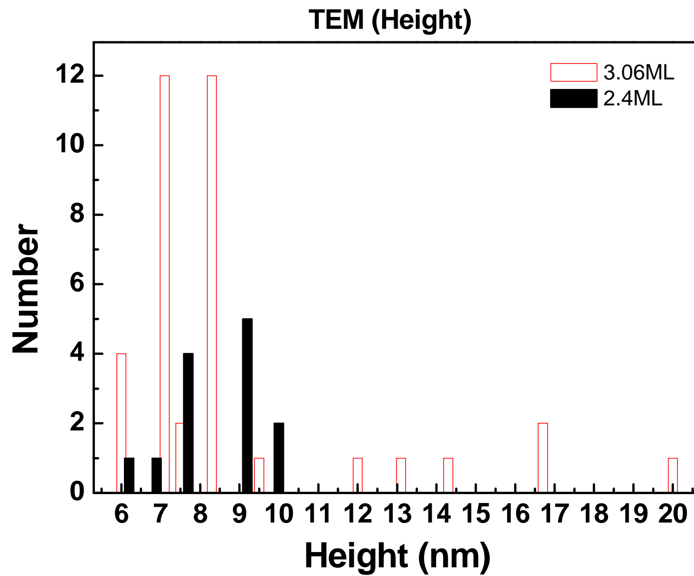

圖 2-2 (a)　2.4 ML 與 3.06 ML 雙模態量子點之高度統計圖

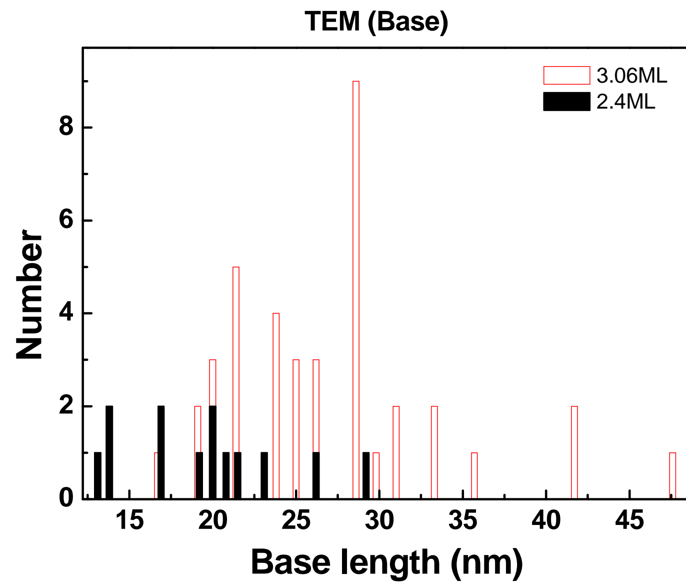

圖 2-2 (b)　2.4 ML 與 3.06 ML 雙模態量子點之基底寬度統計圖

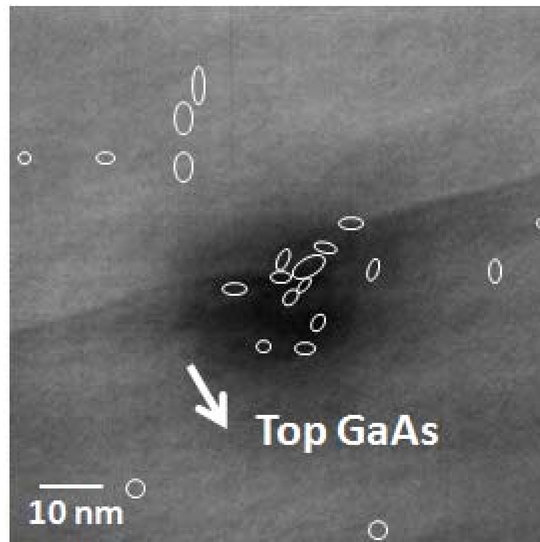

圖 2-3 (a)　3.06 ML 非一致性量子點傳立葉轉換缺陷分析

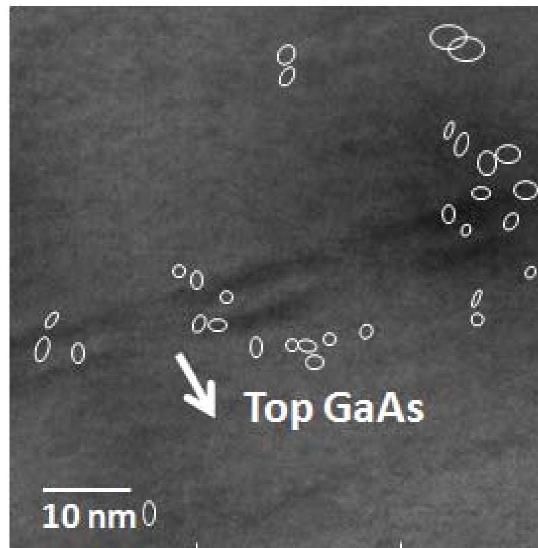

圖 2-3 (b)　3.06 ML 一致性量子點傅立葉轉換缺陷分析

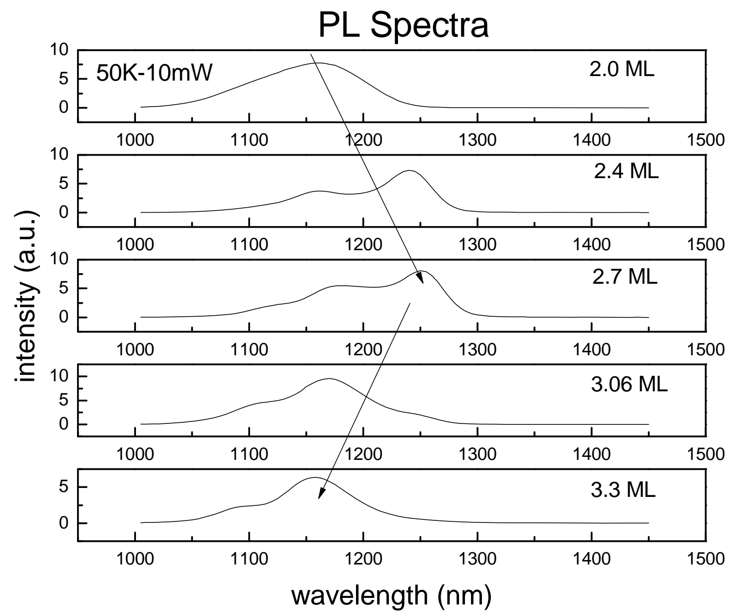

圖 2-4　低溫 50 K 不同厚度量子點樣品 PL 光譜圖

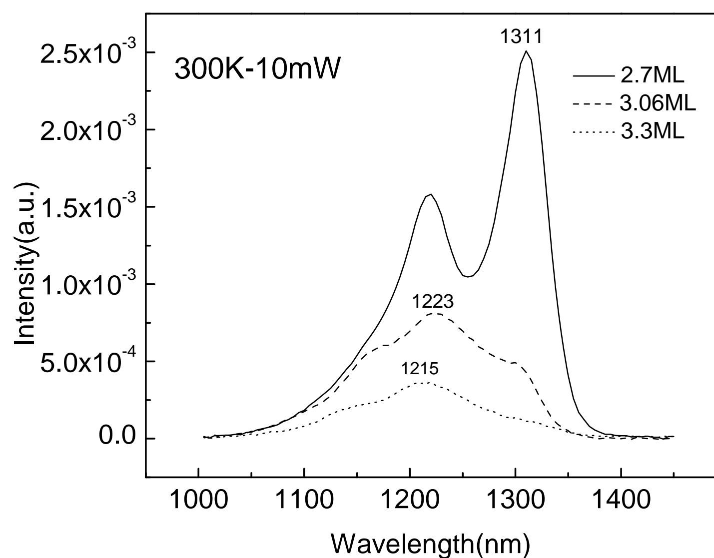

圖 2-5　室溫 300 K 不同厚度量子點樣品 PL 光譜圖

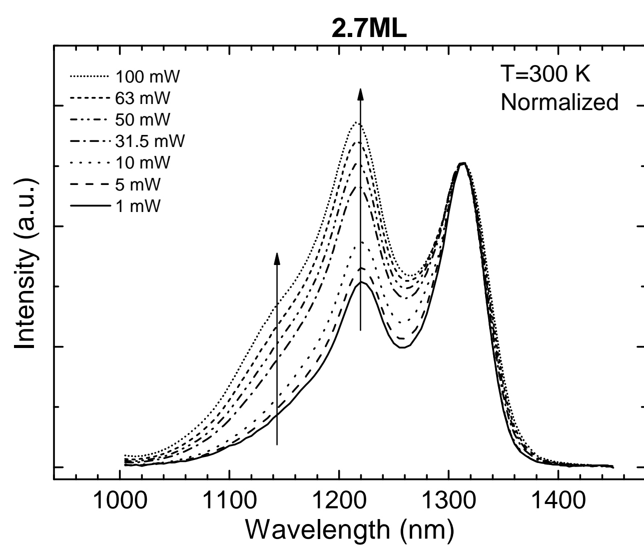

圖 2-6 (a)　2.7 ML 樣品室溫變激發功率 PL 光譜圖

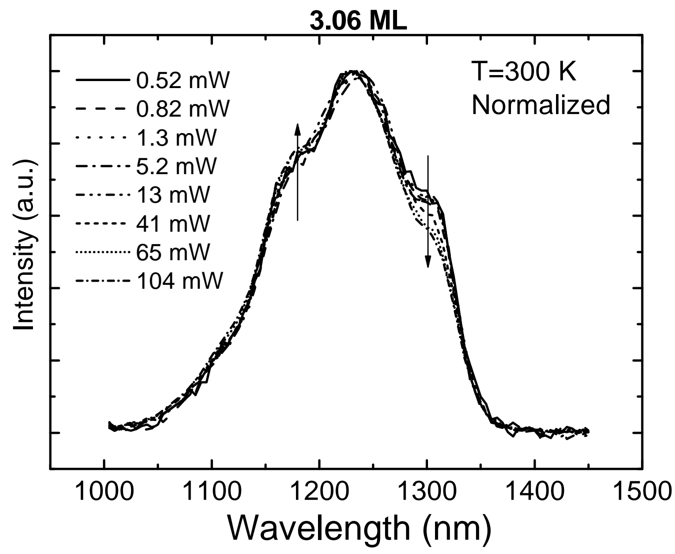

圖 2-6 (b) 3.06 ML 樣品室溫變激發功率 PL 光譜圖

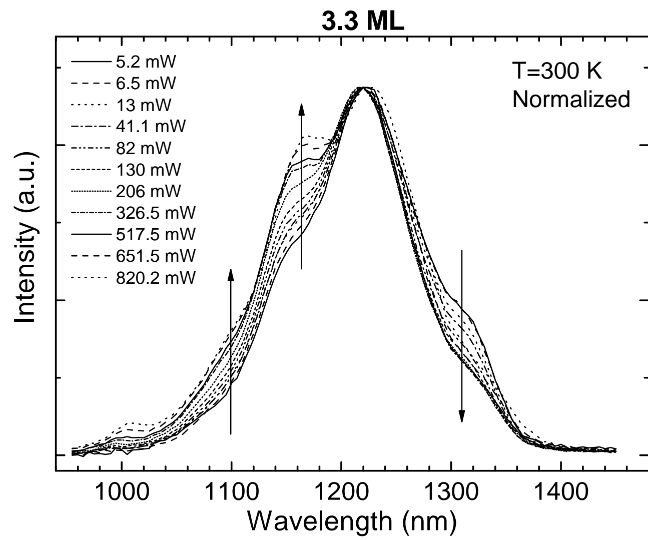

圖 2-6 (c) 3.3 ML 樣品室溫變激發功率 PL 光譜圖。

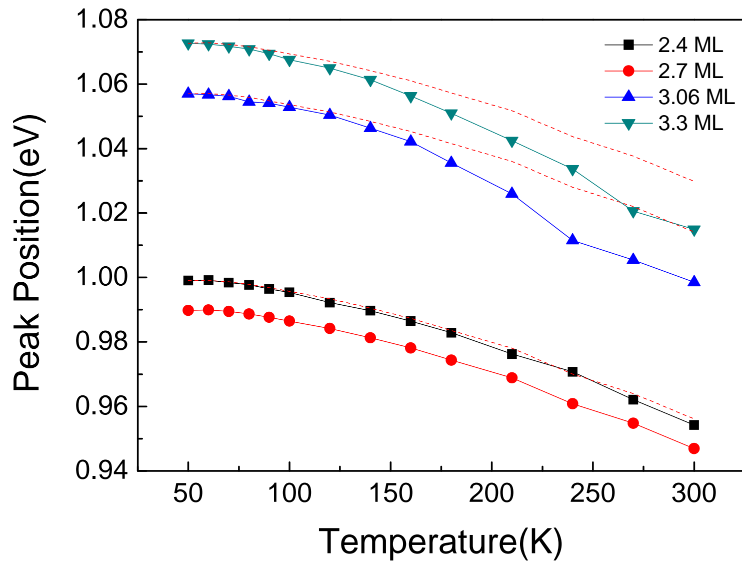

圖 2-7　不同厚度的量子點樣品發光峰值能量變溫圖

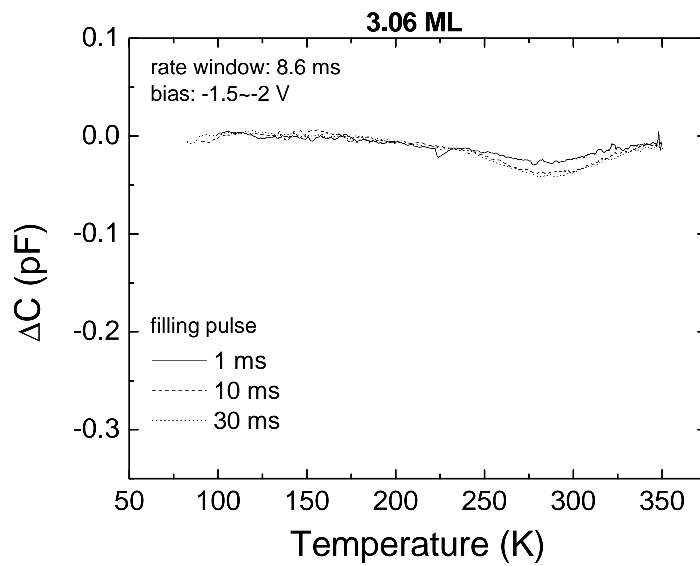

圖 2-8 (a)　3.06 ML 樣品固定偏壓與 rate window 下變 filling pulse 圖

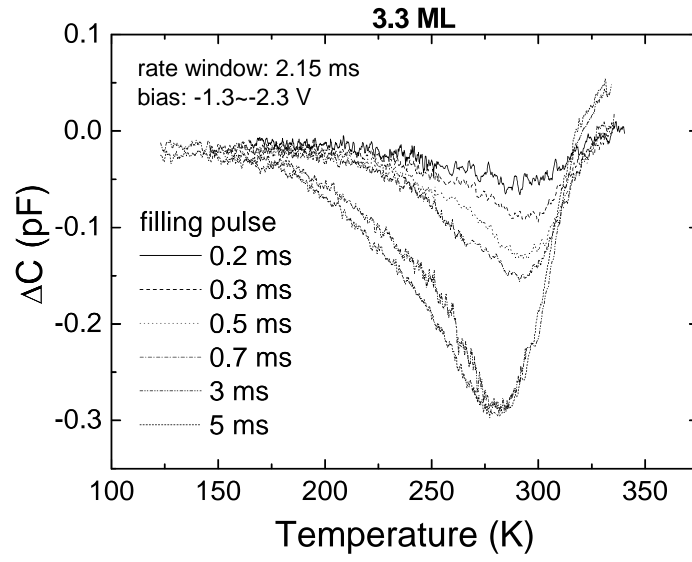

圖 2-8 (b)　3.3 ML 樣品固定偏壓與 rate window 下變 filling pulse 圖

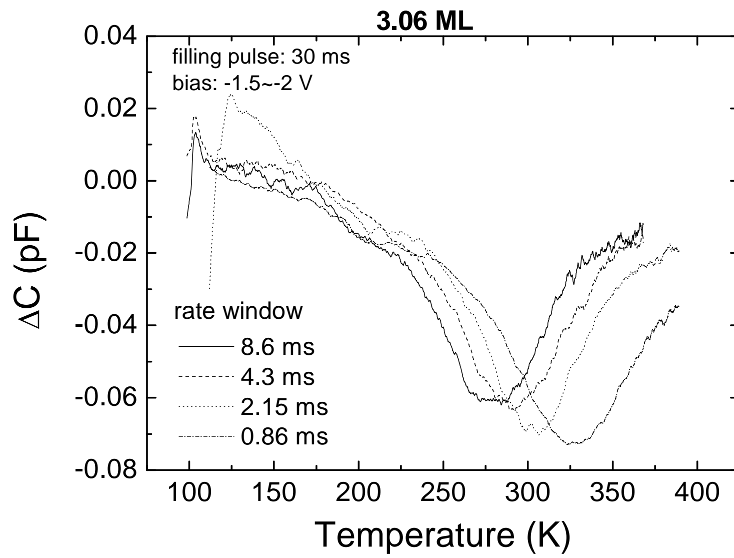

圖 2-9 (a)　3.06 ML 樣品固定偏壓與 filling pulse 下變 rate window 圖

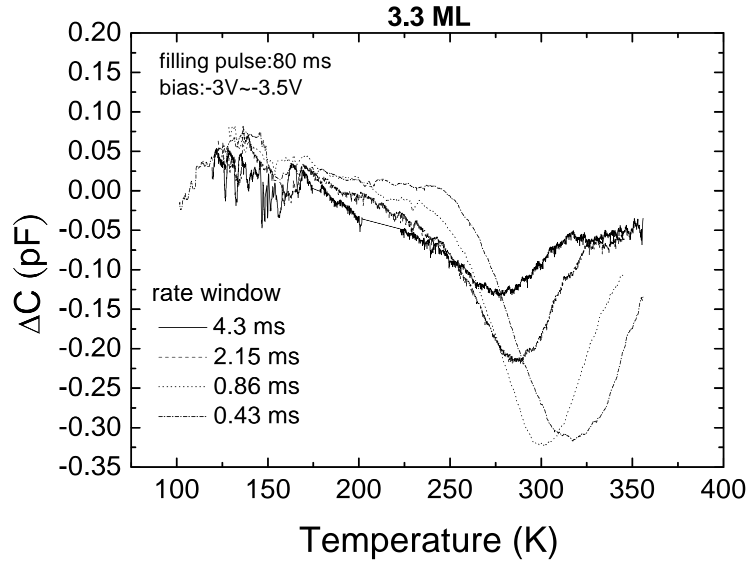

圖 2-9 (b)　3.3 ML 樣品固定偏壓與 filling pulse 下變 rate window 圖

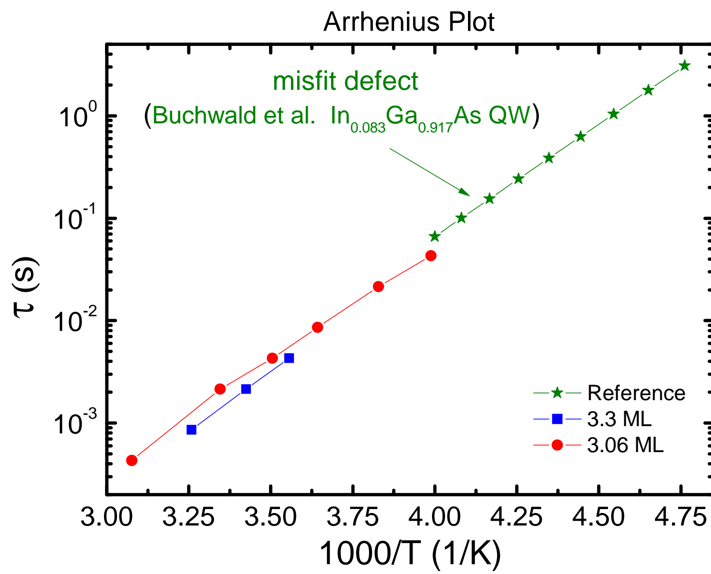

圖 2-10　不圖厚度樣品與 Reference 樣品的阿瑞尼士圖

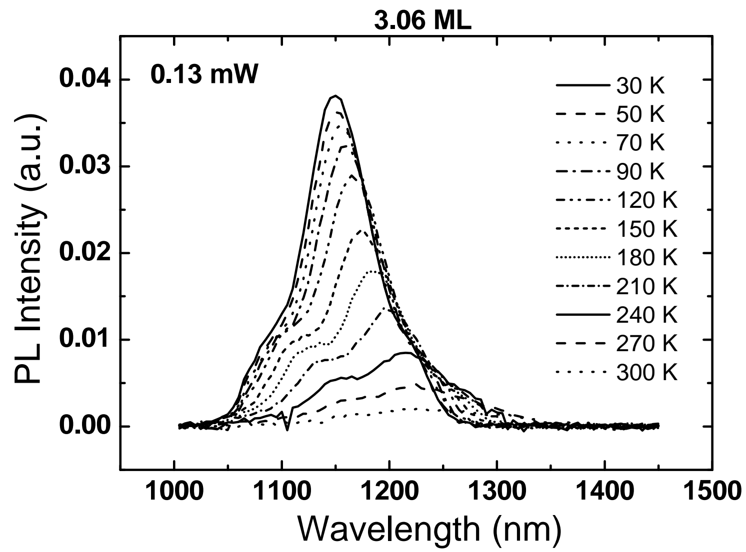

圖 3-1　3.06 ML 樣品溫度相依 PL 光譜圖

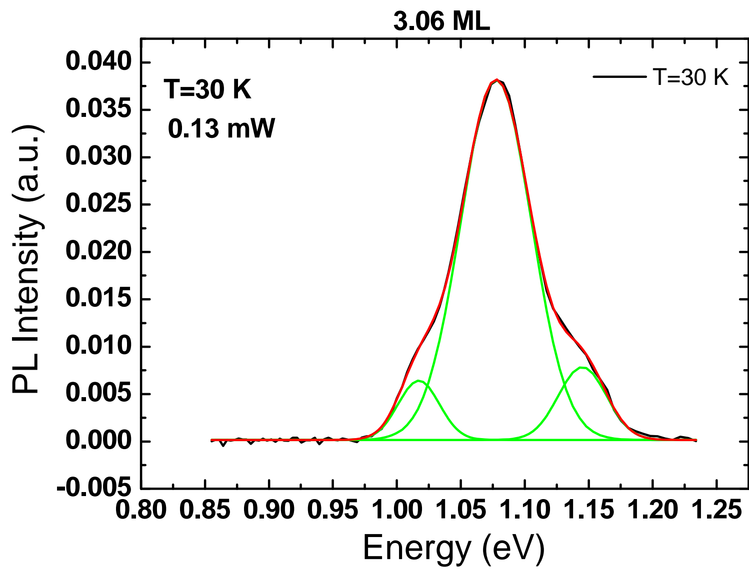

圖 3-2 (a)　3.06 ML 樣品溫度 30 K PL 光譜高斯擬合圖

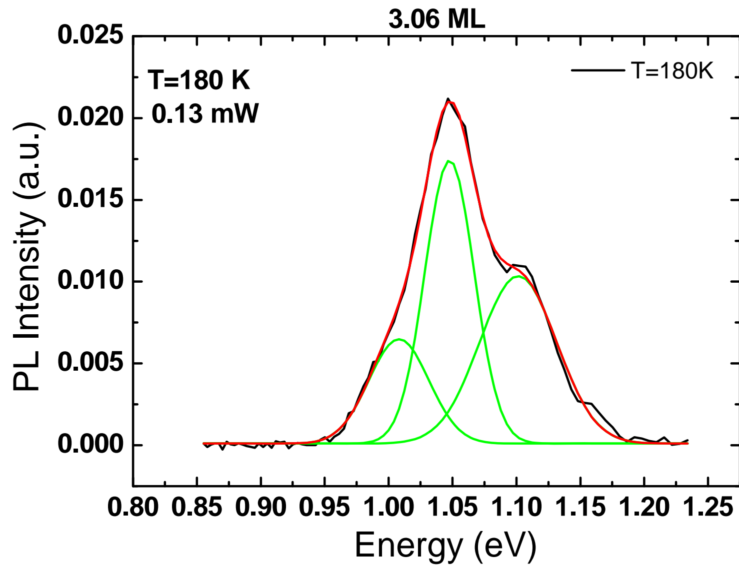

圖 3-2 (b)　3.06ML 樣品溫度 180K PL 光譜高斯擬合圖

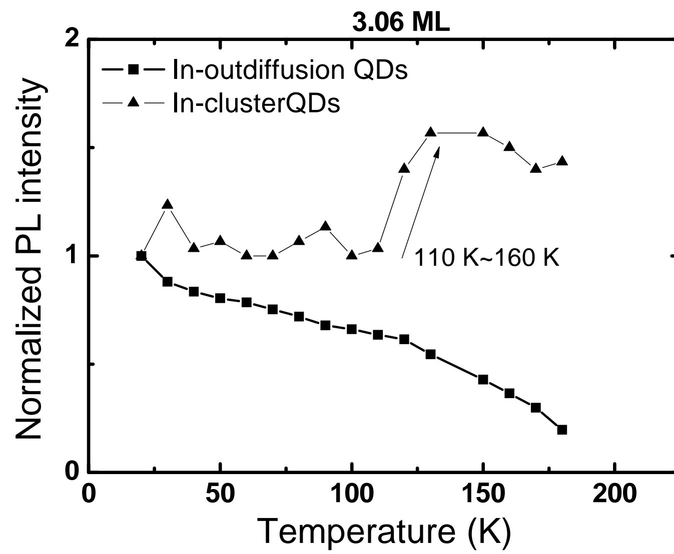

圖 3-3　3.06 ML 樣品溫度相依歸一化 PL 強度圖

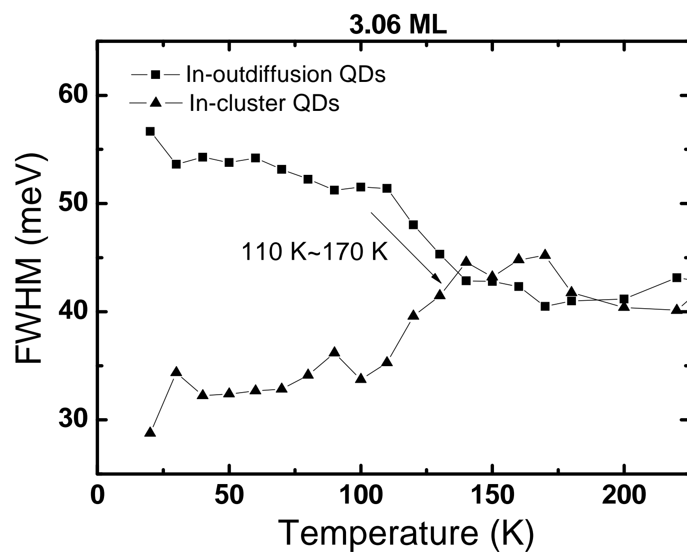

圖 3-4　3.06 ML 樣品溫度相依半高寬圖

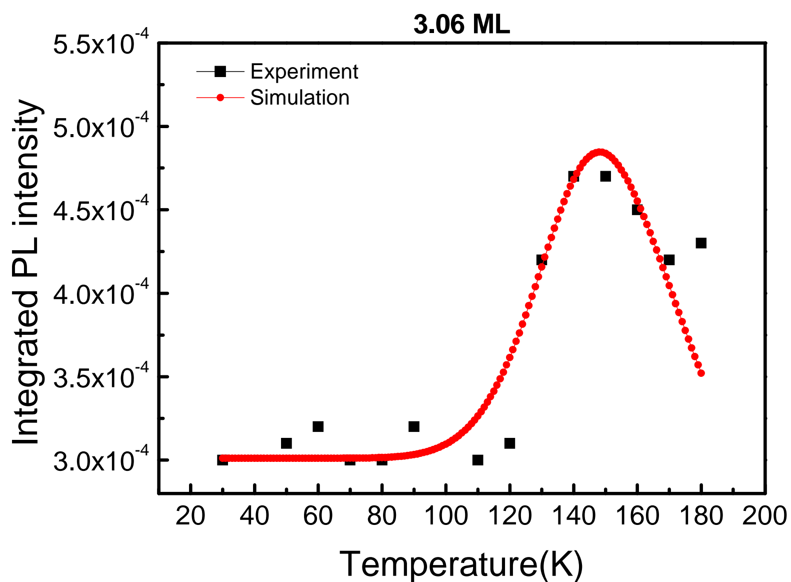

圖 3-5　3.06ML 樣品溫度相依積分強度公式擬合圖

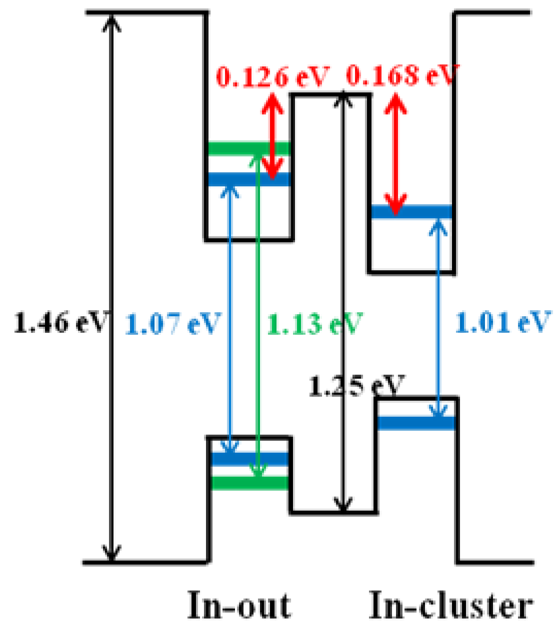

圖 3-6　3.06 ML 樣品溫度 110K 能帶圖(CB:VB=7:3)

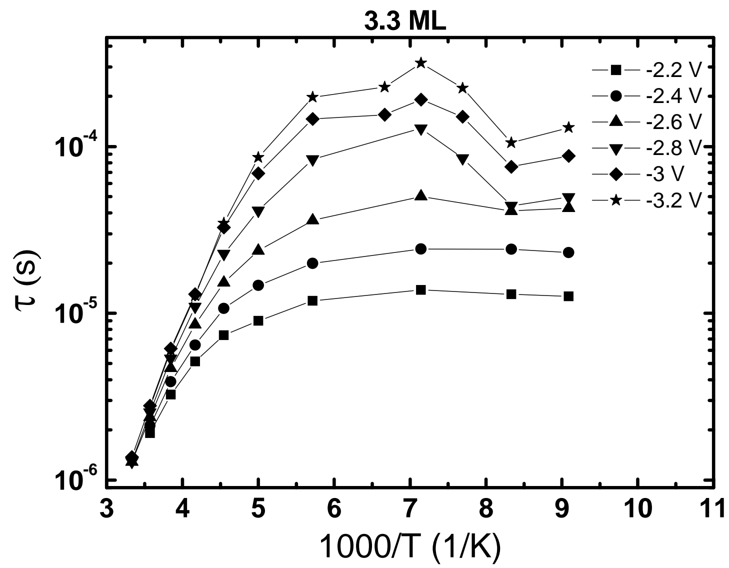

圖 3-7　3.3 ML 樣品各偏壓下的阿瑞尼士圖

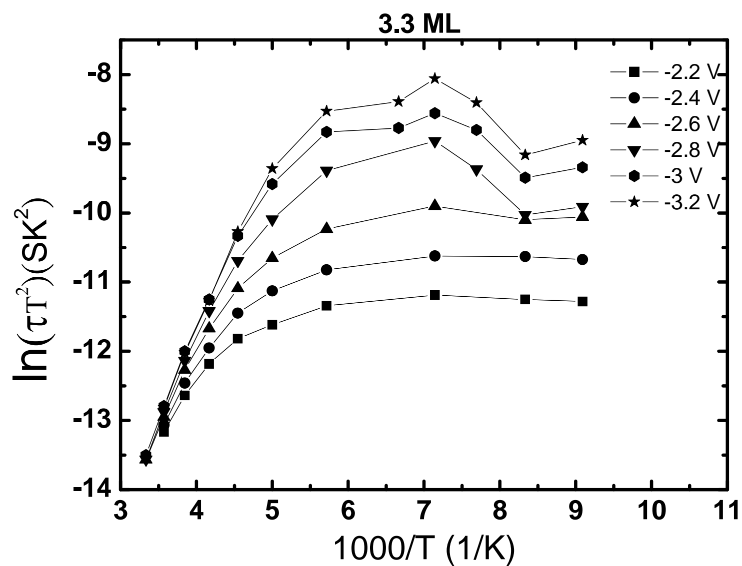

圖 3-8　3.3 ML 樣品各偏壓下的阿瑞尼士圖

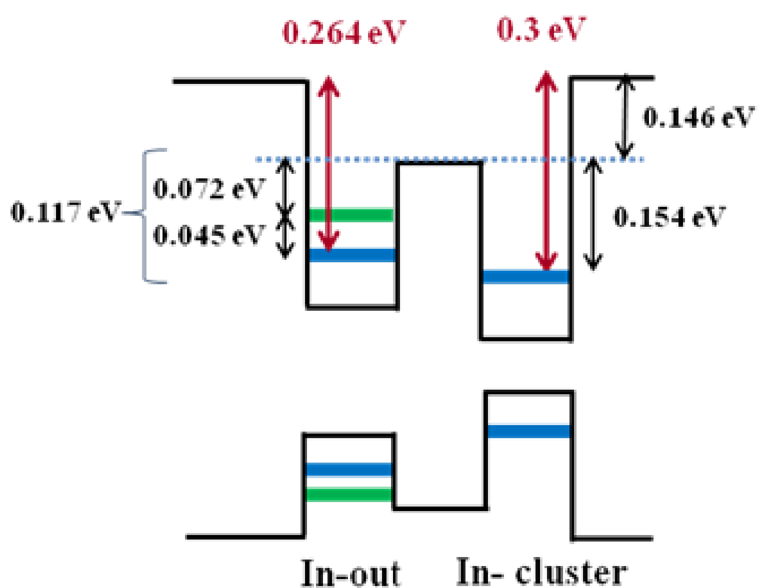

圖 3-9　3.3 ML 樣品溫度 110K 能帶圖(CB:VB=7:3)

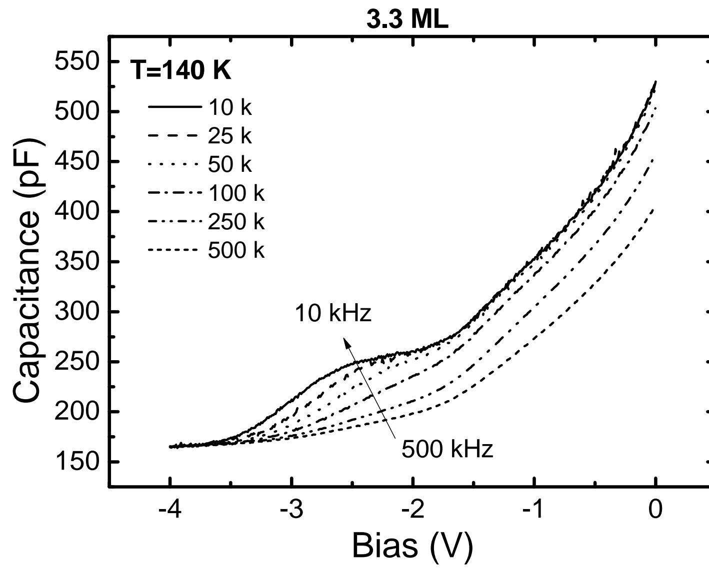

圖 3-10　3.3 ML 樣品定溫 140K 變頻 C-V 圖

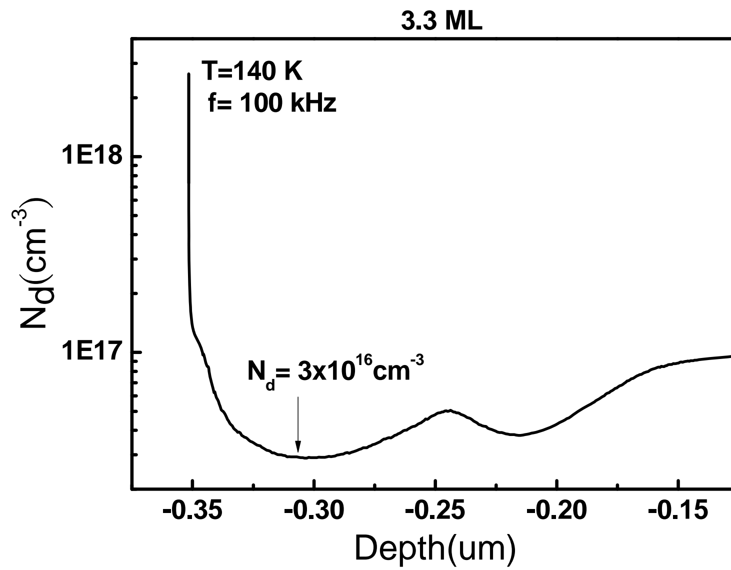

圖 3-11　3.3 ML 樣品溫度 140 K 頻率 100 kHz 轉縱深圖

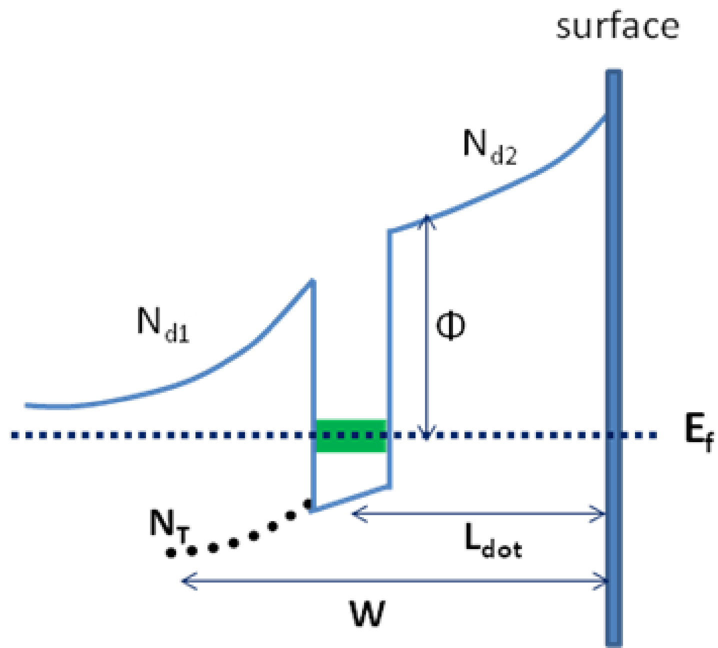

圖 3-12　3.3 ML 樣品模擬能帶示意圖

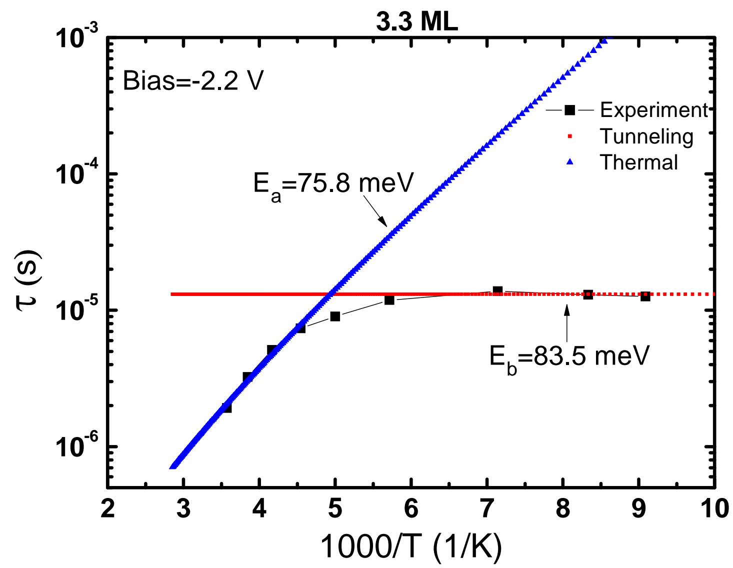

圖 3-13 (a)　3.3 ML 樣品偏壓-2.2 V 兩段式模擬載子躍遷速率圖

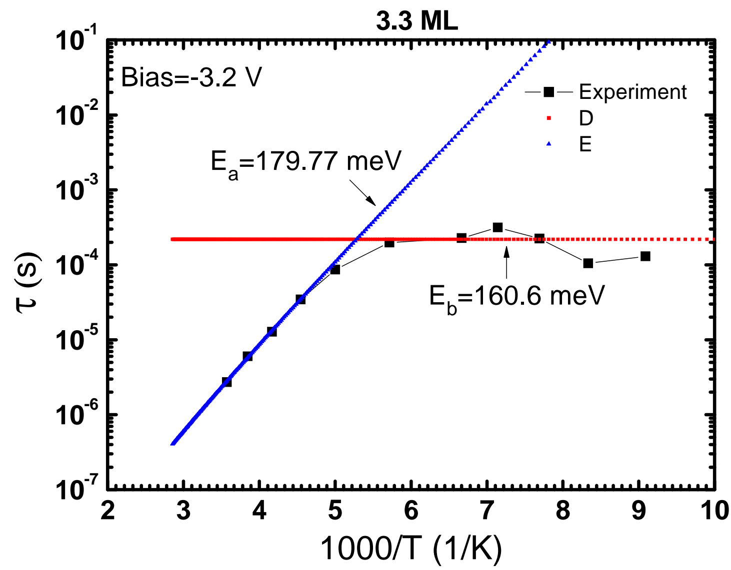

圖 3-13 (b)　3.3 ML 樣品偏壓-3.2 V 兩段式模擬載子躍遷速率圖

	3.06 ML (-1.5 ~ -2 V)	3.3 ML (-3 ~ -3.5 V)
Activation energy Ea (meV)	380	383
Capture cross section σ (cm^{-2})	7.41E-17	1.42E-16

表 1　3.06 ML 與 3.3 ML 樣品的缺陷活化及與捕捉截面積

Bias (V)	Ea (meV)	Capture Cross section (cm^2)
-2.2	97.55	1.62×10^{-18}
-2.4	115.92	3.1×10^{-18}
-2.6	150.76	1.23×10^{-17}
-2.8	160.03	1.68×10^{-17}
-3.0	180	3.51×10^{-17}
-3.2	179.77	3.42×10^{-17}

表 2　3.3 ML 樣品各偏壓下的活化能與捕捉截面積

V_a	C-V Φ (meV)	G-F Ea (meV)	G-F E_b (meV)
-2.2	73	75.8	83.5
-2.4	116	115.92	100.2
-2.6	167	150.76	116
-2.8	239	160.03	134
-3	306	180	150
-3.2	369	179.77	160

表 3 模擬的電位能與穿隧位能障和活化能的比較表

國科會補助專題研究計畫成果報告自評表

請就研究內容與原計畫相符程度、達成預期目標情況、研究成果之學術或應用價值（簡要敘述成果所代表之意義、價值、影響或進一步發展之可能性）、是否適合在學術期刊發表或申請專利、主要發現或其他有關價值等，作一綜合評估。

1. 請就研究內容與原計畫相符程度、達成預期目標情況作一綜合評估

■ 達成目標

□ 未達成目標（請說明，以 100 字為限）

　　□ 實驗失敗

　　□ 因故實驗中斷

　　□ 其他原因

說明：

2. 研究成果在學術期刊發表或申請專利等情形：

論文：■已發表 □未發表之文稿 □撰寫中 □無

專利：□已獲得 □申請中 ■無

技轉：□已技轉 □洽談中 ■無

其他：（以 100 字為限）

3. 請依學術成就、技術創新、社會影響等方面，評估研究成果之學術或應用價值（簡要敘述成果所代表之意義、價值、影響或進一步發展之可能性）（以 500 字為限）

本研究中對於應力誘發雙模態量子點形成機制之探討，可以為未來在應用雙模態量子點時，提供另外一種不同的雙模態量子點生長方式。相較於傳統的雙模態量子點生長方式，應力誘發雙模態量子點之生長方式可以有效地簡化雙模態量子點的生長過程，並且可以達到與傳統生長方式相同特性之雙模態量子點。在應用面上，對於雙模態量子點間載子傳輸機制的瞭解，可以為雙模態量子點未來被應用於量子計算時，提供一個完備且清楚的物理模型，此成果有助於發展其應用。同時，我們也將研究成果投稿至 Applied Physics letters 與 Journal of Applied Physics，所幸在去年時皆已被接受且發表(附錄)。對於計畫成果我們相信仍還可以在進一步的探究我們未解決的現象，使得此研究能盡善盡美，最後我們自評優良算是給予我們團隊鼓勵。

附錄

1. J. F. Chen, Ross C. C. Chen, C. H. Chiang, M. C. Hsieh, Y. C. Chang, and Y. F. Chen, “Compensation effect and differential capacitance analysis of electronic energy band structure in relaxed InAs quantum dots,” J. Appl. Phys. **108**, 063705 (2010).

2. J. F. Chen, Ross C. C. Chen, C. H. Chiang, Y. F. Chen, Y. H. Wu, “Bimodel onset strain relaxation in InAs quantum dots with an InGaAs capping layer,” Appl. Phys. Lett. **97**, 092110 (2010).

Compensation effect and differential capacitance analysis of electronic energy band structure in relaxed InAs quantum dots

J. F. Chen,[a)] Ross C. C. Chen, C. H. Chiang, M. C. Hsieh, Y. C. Chang, and Y. F. Chen
Department of Electrophysics, National Chiao Tung University, Hsinchu, Taiwan 30050, Republic of China

(Received 25 March 2010; accepted 29 June 2010; published online 17 September 2010)

The use of a differential capacitance technique for analyzing the effect of strain relaxation on the electronic energy band structure in relaxed InAs self-assembled quantum dots (QDs) is presented. Strain relaxation is shown to induce a deep defect state and compensate the ionized impurity in the bottom GaAs layer, leading to a double depletion width and a long emission time. An expression of capacitance at different frequency and voltage is derived for analyzing the experimental data. It has been shown that the relationship between the low-frequency and high-frequency capacitances can be well explained by a Schottky depletion model with a compensated concentration in the bottom GaAs layer. A simple expression is presented to account for the modulation of the free electrons in the top GaAs layer. This capacitance analysis shows a long low-energy tail for the electron ground state, suggesting not very uniform strain relaxation. The results of this study illustrate a carrier compensation effect of the defect state on the electronic energy band structure near the QDs.
© *2010 American Institute of Physics*. [doi:10.1063/1.3467938]

I. INTRODUCTION

Understanding the energy band structure in InAs self-assembled quantum dots (QDs) (Refs. 1–15) is important for designing the QD devices such as photodetectors[13,14] or memory devices. In self-assembled InAs QDs, strong strain is built up in the QDs and neighboring GaAs layers. Previous experiments have shown pronounced tunneling emission for the electrons in the QDs escaping to the GaAs.[9–11,16,17] The built-up strain is expected to have a strong effect on the energy band structure and emission mechanism of the QDs. Recently, a significantly elongated electron emission time was observed in strain relaxed QDs.[18] Strain relaxation in the QDs can lead to the generation of threading dislocations in the top GaAs layer and lattice misfits near the QDs.[19] Capping the QDs with an InGaAs strain-relieving layer, strain relaxation in the QDs can be accommodated by the lattice misfits near the QDs and the top GaAs layer is dislocation-free.[18] Most of the lattice misfits were observed in the bottom GaAs layer under the QDs by transmission electron microscopy,[18] suggesting strain relaxation through the bottom GaAs layer. A relaxation-induced defect state at 0.37 eV has been observed in the bottom GaAs layer.[19] Understanding the energy band structure in the relaxed QDs is believed to shed light on the strain effect in the coherently strained QDs. Thus, in this paper, we have derived an expression of capacitance at different frequency and voltage to analyze the electronic band structure in the relaxed QDs. We found that the relaxation-induced defect state can compensate the background ionized impurity in the bottom GaAs layer, leading to a long emission time. Furthermore, strain relaxation induces a long low-energy tail for the electron ground state (EGS) of the QDs, consistent with optical spectra. We showed that the energy band structure near the QDs can be well described by a Schottky depletion mode with a compensated background concentration in the bottom GaAs layer.

II. THEORY

A. Theory of capacitance-voltage (*C-V*) spectra

Based on experimental results, Fig. 1 shows a simplified electron energy band diagram where Fermi level is intersecting with a QD state for a carrier modulation. A relaxation-induced defect state at an energy below the QDs in the GaAs bottom layer is shown. This defect state can trap electrons and compensate the background concentration in the GaAs bottom layer from ionized impurity N_D to a compensated background concentration $N_D' = N_D - N_t$, assuming a uniform N_t in the bottom GaAs layer for simplicity. This compensa-

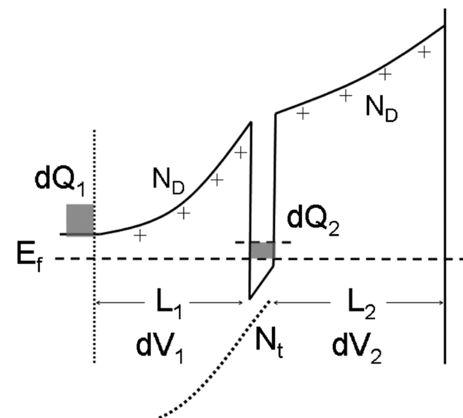

FIG. 1. Simplified electronic energy band diagram for a Schottky diode containing a QD layer for illustrating the modulation of the carriers dQ_1 at the edge of the depletion region and the carriers dQ_2 in the QDs at a confinement energy E. A relaxation-induced defect state N_t is shown in the GaAs bottom layer.

[a)]Electronic mail: jfchen@cc.nctu.edu.tw.

 © 2010 American Institute of Physics

Downloaded 18 Oct 2011 to 140.113.20.108. Redistribution subject to AIP license or copyright; see http://jap.aip.org/about/rights_and_permissions

tion can effectively broaden the depletion region in the bottom GaAs layer near the QDs and suppress the tunneling emission. Applying a small change in the reverse voltage dV can modulate the carriers (per unit area) dQ_1 at the edge of the depletion region and the carriers (per unit area) dQ_2 in the QDs at a confinement energy E. From Gauss's law, dV can be expressed by the sum of the voltage changes across the two regions with their respective widths L_1 and L_2 as follows:

$$dV = dV_1 + dV_2 = \left(\frac{dQ_1}{\boldsymbol{\varepsilon}}\right)L_1 + \left(\frac{dQ_1 + dQ_2}{\boldsymbol{\varepsilon}}\right)L_2,$$

where $\boldsymbol{\varepsilon}$ is the permittivity of the semiconductor. In a similar way as derived previously,[20] $dQ_1 = \boldsymbol{\varepsilon} dV_1 / L_1$ is substituted into the above expression to obtain the ratio of the bias change across L_1 to the total bias change as expressed by

$$\frac{dV_1}{dV} = \frac{L_1}{(L_1 + L_2) + \dfrac{dQ_2}{dV_1}\dfrac{L_1 L_2}{\boldsymbol{\varepsilon}}}.$$

This bias ratio is related to the occupied density of states of the QDs, $dQ_2/dV_1 \equiv C_Q$. This density of states is related to capacitance as expressed by

$$C_L = \frac{dQ_1 + dQ_2}{dV} = \frac{dQ_1}{dV} + \frac{dQ_2}{dV} = \frac{dV_1}{dV}\frac{\boldsymbol{\varepsilon}}{L_1} + \frac{dQ_2}{dV_1}\frac{dV_1}{dV}$$
$$= \frac{(C_1 + C_Q)C_2}{(C_1 + C_Q) + C_2},$$

where $C_1 = \boldsymbol{\varepsilon}/L_1$ and $C_2 = \boldsymbol{\varepsilon}/L_2$ are the geometric capacitance per unit area across L_1 and L_2. This equation states that the capacitance is a parallel combination of C_1 and C_Q followed by a series combination with C_2. This shall be the low-frequency capacitance C_L if the QD electrons can follow the frequency to be modulated. Under a high frequency where the QD electrons cannot be modulated, $C_Q = 0$ and the capacitance is reduced to $C_H = C_1 C_2/(C_1 + C_2) = \varepsilon/(L_1 + L_2)$. Thus, the high-frequency capacitance can be used to obtain L_1 (L_2 is the designated spatial position the QDs). Substituting L_1 into a Schottky depletion model yields the confinement energy E of the probed QD electrons as

$$E = V_1 + \phi_n = (q/2\boldsymbol{\varepsilon})N'_D L_1^2 + (kT/q)In(N_C/N_D), \tag{1}$$

here N'_D is the compensated concentration in the bottom GaAs layer and N_c is the effective density of states in the GaAs conduction band (CB). The applied reverse voltage V_R is related to L_1 by the voltage drop expression: $V_R = V_1 + V_2 - V_{bi}$, where

$$V_1 = (q/2\varepsilon)N'_D L_1^2 \quad \text{and} \quad V_2 = (q/\varepsilon)N'_D L_1 L_2$$
$$+ (q/2\varepsilon)N_D L_2^2 - (L_2/\varepsilon A)\int_{-\infty}^{E} C_Q dE, \tag{2}$$

here V_{bi}(=0.8 eV) is the Schttoky barrier height of the GaAs and $A = 5 \times 10^{-3}$ cm^2 is the area of the diode studied here. The last term in V_2 is the voltage drop due to the occupied electrons in the QDs below Fermi level. For simplicity, we have neglected the Fermi–Dirac distribution.

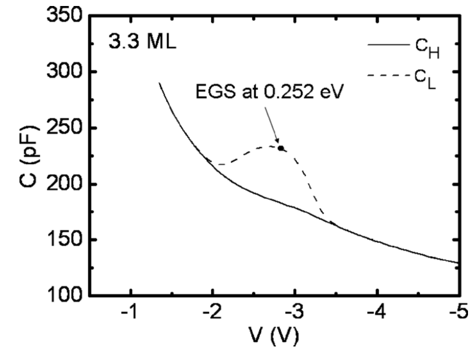

FIG. 2. Simulated low-frequency and high-frequency *C-V* spectra for a Gaussian carrier distribution $C_Q(E)$ at a depth of 0.2 μm at E=0.252 eV with a broadness of 70 meV. The low-frequency spectra display a C protrusion peaked at −2.8 V.

Figure 2 shows simulated *C-V* spectra for a Gaussian carrier distribution $C_Q(E)$ to represent an electron state in the QD with a peak of 680 pF ($=8.6 \times 10^{11}$/cm^2,eV) at E =0.252 eV with a broadness of 70 meV. This carrier distribution $C_Q(E)$ gives a total carrier density of 7.9 $\times 10^{10}$ cm^{-2}, which is close to double the QD density corresponding to a capture of two electrons for an EGS. The simulation uses $N_D = 1 \times 10^{17}$ cm^{-3} and $N'_D = N_D - N_t = 2.9 \times 10^{16}$ cm^{-3} based on the experimental data to be shown. The simulated C_L displays a protrusion from −2 to −3.5 V with a peak at −2.8 V, corresponding to the modulation of the peak of $C_Q(E)$ at E=0.252 eV.

We would like to emphasize that the above derivation works for large amplitude of reverse voltage so that the top GaAs layer is totally depleted of free electrons. For small amplitude of reverse voltage, Fermi level also modulates the free electrons in the top GaAs layer and introduce additional capacitance $C_{\mathrm{GaAs}} = dQ_{\mathrm{GaAs}}/dV_1$, where Q_{GaAs} is the modulated electron density in the top GaAs layer and shall be approximately proportional to the free carrier concentration at the GaAs CB near the QDs, $n_o = N_C \exp(-V_1/kT)$ here $V_1 = (q/2\boldsymbol{\varepsilon})N'_D L_1^2$. Decreasing reverse voltage will increase V_1 to deplete Q_{GaAs} by $Q_{\mathrm{GaAs}} = Q_{\mathrm{GaAs},o}\exp(-V_1/kT)$. Accordingly, this additional capacitance rapidly decreases with increasing V_1 by $C_{\mathrm{GaAs}} = dQ_{\mathrm{GaAs}}/dV_1 = (1/kT)Q_{\mathrm{GaAs}} = C_{\mathrm{GaAs},o}\exp(-V_1/kT)$. This effect is appreciable only when $V_1(L_1)$ is very small. Under this condition, the modulated free carriers are nearly at the same spatial location as the QDs, leading to the low-frequency capacitance can be approximately expressed by $C_L \cong C_2 + C_Q + C_{\mathrm{GaAs}}$ while $C_H \cong C_2$. Thus, the effect of the carrier modulating in the top GaAs layer can be simply removed by subtracting $C_{\mathrm{GaAs}} = C_{\mathrm{GaAs},o}\exp(-V_1/kT)$ from C_L. This effect, if not removed, would lead to an overestimation of the carrier density in the shallow QD electrons. This free carrier modulation effect is significant in the relaxed QDs because of the broad carrier depletion near the QDs.

III. MEASUREMENT AND RESULTS

The InAs QD samples were grown by solid source molecular beam epitaxy in a Riber machine. On top of a n$^+$-GaAs(100) substrate, a 0.3 μm-thick Si-doped GaAs (

Downloaded 18 Oct 2011 to 140.113.20.108. Redistribution subject to AIP license or copyright; see http://jap.aip.org/about/rights_and_permissions

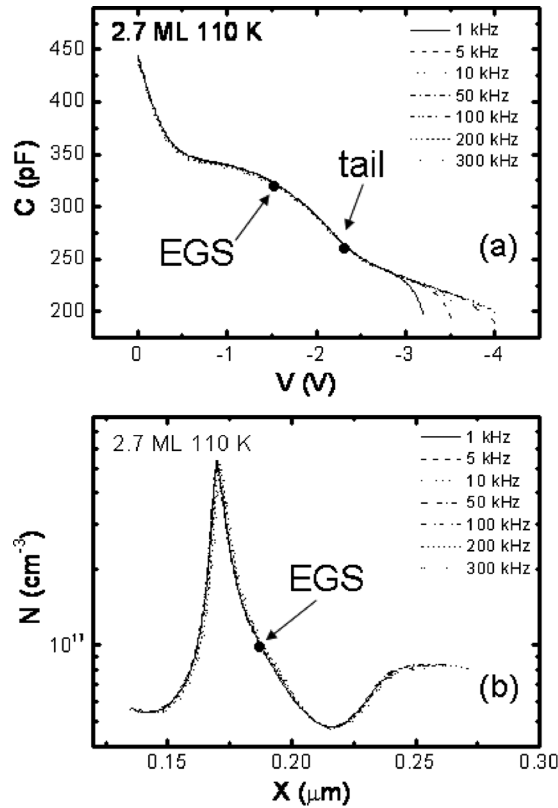

FIG. 3. (a) 110 K *C-V* and (b) the converted carrier distribution for a nonrelaxed QD diode with InAs deposition thickness of 2.7 ML, illustrating a *C* plateau from −0.5 to −2.5 V related to the modulation of the QD electrons.

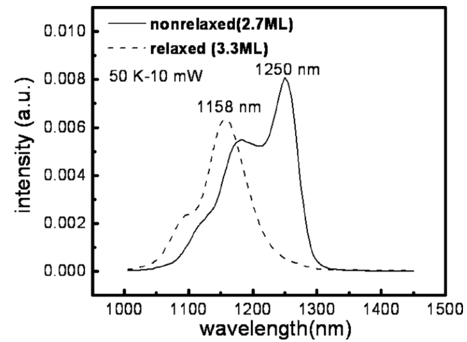

FIG. 4. 50 K PL spectra for nonrelaxed QDs with InAs deposition thickness of 2.7 ML and relaxed QDs with InAs deposition thickness of 3.3 ML. Strain relaxation causes a blueshift in the ground emission and produces a long low-energy tail.

$\sim 1\times 10^{17}$ cm^{-3}) barrier layer, an InAs layer with different deposition thickness from 2 to 3.3 monolayer (ML) was deposited at 490 °C (at a rate of 0.26 Å/s) to form the QDs. Following the growth of the QDs layer, a 60 Å $In_{0.15}Ga_{0.85}As$ strain-relieving capping layer and a 0.2 μm-thick Si-doped GaAs ($\sim 10^{17}$ cm^{-3}) barrier layer were grown to terminate the growth. Relaxation in the QDs was achieved by increasing the InAs deposition thickness slightly beyond a critical thickness about 3 ML. A photoluminescence (PL) blueshift[21] about 80 meV is observed when strain relaxation in the QDs occurs. The QD sheet density is estimated to be $\sim 3\times 10^{10}$ cm^{-2} from performing atomic force microscopy on sample surface where a layer of similar QDs was purposely grown. For *C-V* profiling, Schottky diodes were realized by evaporating Al on sample surface with an area 5×10^{-3} cm^2. A HP 4194A impedance analyzer was used for *C-V* measurements with an oscillation level set at 50 mV.

A. *C-V-F* spectra

1. Coherently strained QDs

Figures 3(a) and 3(b) shows the 110 K *C-V* and its converted carrier distribution using:$N(w)=(C^3/q\varepsilon\varepsilon_0(dC/dV))$ for a nonrelaxed QD diode with InAs deposition thickness of 2.7 ML. A *C* plateau from −0.5 to −2.5 V, corresponding to the modulation of the QD electrons, is visible. This plateau can be dissolved into a peak and a shoulder in the carrier distribution plot. The peak is attributed to the QD first excited state and the shoulder to the EGS of the QDs. When temperature is lowered to 90 K, the shoulder displays frequency dispersion with an activation energy about 60 meV, suggesting a tunneling emission through the first excited state.[18] The emission energy of the first-excited state cannot be obtained from the *C-V* spectra because no frequency dispersion is observed (the emission time is very short). We can estimate the confinement energy for the tail of the EGS because, at this nearly ending of modulation, the low-frequency capacitance shall approach the high-frequency capacitance. Let us choose $C=245$ pF at −2.5 V as the tail of the QDs. This C gives $L_1+L_2=0.234$ μm ($L_2=0.16$ μm is the designed QDs position from the surface). Substituting $L_1=0.074$ μm and a $N_D=8\times 10^{16}$ cm^{-3} for N_D'(seen in the carrier distribution) into Eq. (1) yields $E=0.320$ eV (at 110 K). As shown in Fig. 4, the 50 K PL spectra of this sample show a ground emission at 1250 nm (0.992 eV) with a narrow full width at half maximum of 35 meV. If we take this broadness as the broadness of the EGS, the EGS shall be at 0.303 eV. This gives the confinement energy of the hole ground state (HGS) of $1.50-0.992-0.303=0.205$ eV, giving rise to a ratio of the confinement energy of EGS to HGS of 0.60 to 0.40, a value close to a previously reported 0.61:0.39.[22] The confinement energy of the EGS in the relaxed QDs shall be slightly smaller than that (0.303 eV) of the nonrelaxed QDs because the PL spectra show a blueshift of 79 meV when the relaxation occurs.[21] Figure 4 shows the PL ground emission at 1.071 eV for the relaxed QDs. This blueshift could move the EGS to 0.256 eV in the relaxed QDs assuming the above ratio of 0.6:0.4. This rough estimation shows that the EGS of the relaxed QDs shall be around 0.256 eV.

2. Relaxed QDs

Figures 5(a) and 5(b) show the 110 K *C-V* and the converted carrier distribution for a relaxed QD diode with InAs deposition thickness of 3.3 ML. Its 50 K PL spectra are shown in Fig. 4. The *C-V* spectra display two *C* plateaus. The plateau from −1.5 to −3.4 V is attributed to the QD electrons since its converted carrier profiling displays a similar feature as observed in the nonrelaxed QDs as follows: a peak at 0.217 μm from the first excited state (the QD spatial position is designed at 0.2 μm), and a shoulder at 0.225 μm from the EGS. In contrast to no frequency dispersion observed in the nonrelaxed QDs, the *C-V* spectra of the relaxed

Downloaded 18 Oct 2011 to 140.113.20.108. Redistribution subject to AIP license or copyright; see http://jap.aip.org/about/rights_and_permissions

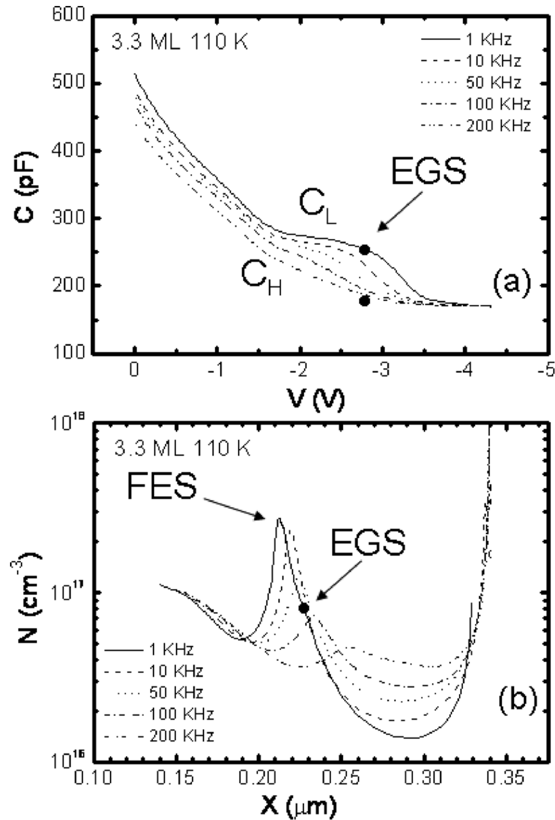

FIG. 5. (a) 110 K *C-V* and (b) the converted electron distribution for a relaxed QD diode with InAs deposition thickness of 3.3 ML. The *C* plateau from −1.5 to −3.4 V is related to the modulation of the QD electrons and the *C* plateau starting from −3.5 V is related to the relaxation-induced defect state.

QDs display frequency dispersion, suggesting a longer emission time. As shown in Fig. 5(a), the *C* protrusion diminishes with increasing frequency, reflective of an incapability of carrier modulation. Note that we observed no appreciable change in the *C-V* spectra when frequency is lower than 1 kHz or higher than 200 kHz, and thus we take *C* at 1 kHz as C_L and at 200 kHz as C_H for the following analysis. The 0.217 μm (at −2.54 V) for the first excited state and the 0.225 μm (at −2.8 V) for the EGS cannot be interpreted as the positions of the edge of the depletion region because the concentration profiling in Fig. 5(b) is converted from the low-frequency capacitance which is affected by the modulation of the QDs. We should use the high-frequency capacitance. Figure 5(a) shows C_H=196 pF at −2.54 V (186 pF at −2.8 V), which gives L_1+L_2=0.293 μm (0.308 μm). After substituting from L_2=0.2 μm (the QDs position from the surface), we obtain L_1=0.093 μm (0.108 μm). Substituting these L_1 and $N_D'=2.9\times10^{16}$ cm^{-3} (to be determined in a later section) into Eq. (1) yield confinement energies of E =0.189 eV and 0.252 eV for the first-excited state and EGS, respectively. The energy for the EGS is consistent with the one (0.256 eV) estimated from the nonrelaxed QDs. Note that, during the simulation (in Fig. 2), an electron state at 0.252 eV would result in a *C* plateau peaked at −2.8 V.

As shown in Fig. 5(a), the QD plateau is immediately followed by another *C* plateau (starting at −3.5 V) which shows no frequency dispersion, suggesting an emission time too long to be modulated. This plateau is attributed to the relaxation-induced defect state previously identified at 0.37 eV below the GaAs CB by deep-level transient spectroscopy.[19] The nearly voltage-independent capacitance suggests a pinning of Fermi level, implying a density of states being comparable to the background ionized impurity. Figure 5(b) shows drastic carrier depletion after the QD, suggesting a lower background concentration due to the carrier compensation of this defect state. Further decreasing reverse voltage will push down Fermi level to intersect with the defect state, giving rise to the second plateau at −3.5 V (and the converted carrier peak) until all the trapped electrons are swept out of the defect state. This defect state behaves like a point defect state whose properties were previously studied in details.[19] It is similar as the one (0.395 eV, $\sigma=1\times10^{-16}$ cm^2) observed by Uchida *et al.*[23] in strain relaxed InGaAs/GaAs quantum well structures. The fact that the tail of the QD (at −3.4 V) is immediately followed by the defect state stipulates that the tail of the EGS shall have a confinement energy of ~0.37 eV.

B. Compensation of background concentration

One pronounced feature associated with the defect state is the asymmetric carrier distribution on the sides of the QDs, as shown in Fig. 5(b). The top GaAs layer displays a normal carrier depletion near the QDs and a designated background concentration of $N_D=1\times10^{17}$ cm^{-3}. On the other hand, the bottom GaAs layer displays a lower background concentration with a nearly double depletion width, suggesting a compensation of the ionized impurity by the defect state. Based on a simple Schottky depletion model $V=(q/2\varepsilon)N_DL^2$, a double depletion width would require a reduction in the background concentration from 1×10^{17} to 2.5×10^{16} cm^{-3}, leading to an effective trapped concentration $N_t=7.5\times10^{16}$ cm^{-3}.

We can obtain a more accurate compensated concentration N_D' by using the voltage drop relationship: $V_R=V_1+V_2-V_{bi}$ in Eq. (2). At −3.4 V, the QDs are nearly empty of carriers and thus the term $(L_2/\varepsilon A)\int_{-\infty}^{E}C_QdE$ in Eq. (2) can be neglected. Figure 5(a) shows C_H=173 pF at −3.4 V, corresponding to L_1=0.132 μm. Substituting the L_1, L_2 =0.2 μm, V_R=3.4 V and V_{bi}=0.8 V into Eq. (2) gives $N_D'=2.9\times10^{16}$ cm^{-3}. This is close to the value (2.5×10^{16} cm^{-3}) estimated from a double depletion width in the bottom GaAs layer. Substituting this N_D' and L_1=0.132 μm into Eq. (1) yields E=0.364 eV (at 110 K). This energy, obtained from nearly the end of the modulation of the QDs, shall correspond to the tail of the EGS. As mentioned above, this energy shall be close to that of the defect state (0.37 eV) because Fig. 5(a) shows that the tail of the QD is immediately followed by the defect state. This consistency supports the validity of using a compensated concentration in a Schottky depletion model to describe the electronic energy band in the bottom GaAs layer near the QDs. Note that we have used this compensated background concentration $N_D'=2.9\times10^{16}$ cm^{-3} to obtain the confinement energy of the EGS which is E=0.252 eV. This energy and the PL ground emission (1.078 eV at 110 K) results in the confinement en-

Downloaded 18 Oct 2011 to 140.113.20.108. Redistribution subject to AIP license or copyright; see http://jap.aip.org/about/rights_and_permissions

ergy of a HGS of 1.50−1.078−0.252=0.170 eV, giving rise to a ratio of the confinement energy of EGS to HGS of 0.60 to 0.40, in agreement with a ratio obtained from the nonrelaxed QDs. Note that this $N_D'=2.9\times 10^{16}$ cm^{-3} was also used for the simulation in Fig. 2 to produce a C plateau peaked at −2.8 V from an electron state at 0.252 eV.

The EGS at 0.252 eV with its tail at 0.364 eV suggests a tail as wide as 112 meV. A long low-energy tail is also seen in the PL ground emission of the relaxed QDs in Fig. 4, which display a tail extending to about 1300 nm, about 117 meV from the peak of the ground emission at 1.071 eV. Note that this long low-energy tail is not seen in the nonrelaxed QDs, and thus it is related to strain relaxation. Strain relaxation can enhance the fluctuation of the QD states and form a long low-energy tail, suggesting the process is not very homogenous.[19] Note that the carrier compensation effect caused by the relaxation-induced defect state can increase L_1 from 0.074 to 0.132 μm at the tail of the EGS. This, along with the reduction in N_D from 8×10^{16} to 2.9×10^{16} cm^{-3}, would reduce the electric field at the QD from 8.2×10^6 to 5.3×10^6 V/m from the expression $E=(q/\varepsilon)N_D'L_1$. As a result, the tunneling emission is significantly suppressed, resulting in a long emission time in the relaxed QDs.

C. Effect of the free carrier modulation in the top GaAs layer

Probably due to the large L_1, the free electrons in the top GaAs layer when they traverse through the QD region to the bottom GaAs layer will exert an observable time constant. The C-V spectra in Fig. 5(a) display frequency dispersion from 0 to −1.5 V (with a nearly temperature-independent inflexion frequency of about 6×10^5 Hz determined from C-F spectra). As explained in the section of the theory, this is the modulation of the free electrons in the top GaAs layer with $C_L=C_2+C_{\mathrm{GaAs}}$ and $C_H=C_2$. The $C_{\mathrm{GaAs}}=C_L-C_H$ =40 pF at the starting modulation of the QDs (at −1.5 V) gives $Q_{\mathrm{GaAs}}=4.8\times 10^8/\mathrm{cm}^2$ from $C_{\mathrm{GaAs}}=(1/kT)Q_{\mathrm{GaAs}}$. This free-carrier modulation effect if not removed would lead to an overestimation of the electron density for the shallow QD electrons. This modulation diminishes rapidly with reverse voltage by $C_{\mathrm{GaAs}}=C_{\mathrm{GaAs},o}\exp(-V_1/kT)$. For example, this effect decays to e^{-1} when the applied voltage probes the QD electrons at $E=36$ meV ($V_1=9.5$ meV at 110 K). Thus, it affects only the shallow QD electrons. At around −1.5 V, C_1 can be considered not exist ($L_1\to 0$) and $C_L=C_2+C_Q+C_{\mathrm{GaAs}}$ and $C_H=C_2$. Thus, we remove this free carrier modulation effect by subtracting C_L from C_{GaAs} and the result is shown in the dashed curve in Fig. 6. In this figure, we have converted the reverse voltage to the confinement energy E of the QD from the high-frequency capacitance as shown in the inset. From the lowest frequency of 1 kHz which allows the modulation of all the QD electrons, the QD electrons are filled from ~0.38 eV to the GaAs CB edge. In the figure, we have marked the EGS and first excited state of the QDs based on the PL spectra. From $C_L=((C_1+C_Q)C_2/(C_1+C_Q)+C_2)$ shown in the theory, we obtained C_Q and estimated the total electron density about 2×10^{11} cm^{-2}. Thus, each QD contains about eight electrons (QD density=~3 $\times 10^{10}$ cm^{-2}).

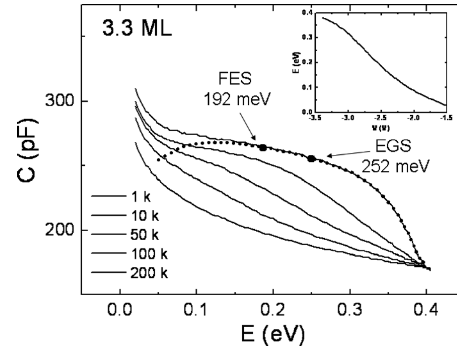

FIG. 6. Measured capacitance vs the confinement energy of the QD electrons converted from Fig. 5(a) using the high-frequency capacitance. The inset shows the converted relationship between reverse voltage and the confinement energy.

IV. CONCLUSIONS

We present a differential capacitance analysis to establish the electronic band structure in strain relaxed InAs QDs. Strain relaxation can introduce a deep defect state to compensate the ionized impurity in the bottom GaAs layer, resulting in a wide depletion width and a long emission time. We show the validity of using a compensated background concentration in a Schottky depletion model to describe the electronic energy band in the GaAs bottom layer. The EGS of the QDs is obtained to be 0.252 eV, giving a ratio of the confinement energies of the electron to HGSs of 0.60 to 0.40. This analysis shows the presence of a long tail for the EGS of the QDs, consistent with the PL spectra.

ACKNOWLEDGMENTS

The authors are grateful to Dr. J. Y. Chi and R. S. Hsiao for sample preparation and would like to thank the National Science Council of the Republic of China, Taiwan for financially supporting this research under Contract No. NSC-97-2112-M-009-014-MY3. This work is partially supported by MOE ATU program.

[1]F. Heinrichsdorff, M. H. Mao, N. Kirstaedter, A. Krost, and D. Bimberg, Appl. Phys. Lett. **71**, 22 (1997).
[2]D. J. Eaglesham and M. Cerullo, Phys. Rev. Lett. **64**, 1943 (1990).
[3]D. Leonard, K. Pond, and P. M. Petroff, Phys. Rev. B **50**, 11687 (1994).
[4]J. M. Moison, F. Houzay, F. Barthe, and L. Leprince, Appl. Phys. Lett. **64**, 196 (1994).
[5]C. W. Snyder, J. F. Mansfield, and B. G. Orr, Phys. Rev. B **46**, 9551 (1992).
[6]H. Shoji, K. Mukai, N. Ohtsuka, M. Sugawara, T. Uchida, and H. Ishikawa, IEEE Photon. Technol. Lett. **7**, 1385 (1995).
[7]G. Yusa and H. Sakaki, Electron. Lett. **32**, 491 (1996).
[8]J. C. Campbell, D. L. Huffaker, H. Deng, and D. G. Deppe, Electron. Lett. **33**, 1337 (1997).
[9]C. M. A. Kapteyn, F. Heinrichsdorff, O. Stier, R. Heitz, M. Grundmann, and P. Werner, Phys. Rev. B **60**, 14265 (1999).
[10]P. N. Brunkov, A. Patane, A. Levin, L. Eaves, P. C. Main, Y. G. Musikhin, B. V. Volovik, A. E. Zhukov, V. M. Ustinov, and S. G. Konnikov, Phys. Rev. B **65**, 085326 (2002).
[11]W. H. Chang, W. Y. Chen, T. M. Hsu, N. T. Yeh, and J. I. Chyi, Phys. Rev. B **66**, 195337 (2002).

Downloaded 18 Oct 2011 to 140.113.20.108. Redistribution subject to AIP license or copyright; see http://jap.aip.org/about/rights_and_permissions

[12] X. Letartre, D. Stievenard, and M. Lanoo, J. Appl. Phys. **69**, 7336 (1991).
[13] H. Drexler, D. Leonard, W. Hansen, J. P. Kotthaus, and P. M. Petroff, Phys. Rev. Lett. **73**, 2252 (1994).
[14] S. Sauvage, P. Boucaud, F. H. Julien, J.-M. Gerard, and J.-Y. Marzin, J. Appl. Phys. **82**, 3396 (1997).
[15] H. L. Wang, F. H. Yang, S. L. Feng, H. J. Zhu, D. Ning, H. Wang, and X. D. Wang, Phys. Rev. **61**, 5530 (2000).
[16] J. Ibáñez, R. Leon, D. T. Vu, S. Chaparro, S. R. Johnson, C. Navarro, and Y. H. Zhang, Appl. Phys. Lett. **79**, 2013 (2001).
[17] J. F. Chen, R. S. Hsiao, C. K. Wang, J. S. Wang, and J. Y. Chi, J. Appl. Phys. **98**, 013716 (2005).
[18] J. F. Chen, Y. Z. Wang, C. H. Chiang, R. S. Hsiao, Y. H. Wu, L. Chang, J. S. Wang, T. W. Chi, and J. Y. Chi, Nanotechnology **18**, 355401 (2007).
[19] J. F. Chen and J. S. Wang, J. Appl. Phys. **102**, 043705 (2007).
[20] J. F. Chen, N. C. Chen, J. S. Wang, and Y. F. Chen, IEEE Trans. Electron Devices **48**, 204 (2001).
[21] J. F. Chen, R. S. Hsiao, Y. P. Chen, J. S. Wang, and J. Y. Chi, Appl. Phys. Lett. **87**, 141911 (2005).
[22] S. D. Lin, V. V. IIchenko, V. V. Marin, K. Y. Panarian, A. A. Buyanin, and O. V. Tretyak, Appl. Phys. Lett. **93**, 103103 (2008).
[23] Y. Uchida, H. Kakibayashi, and S. Goto, J. Appl. Phys. **74**, 6720 (1993).

Downloaded 18 Oct 2011 to 140.113.20.108. Redistribution subject to AIP license or copyright; see http://jap.aip.org/about/rights_and_permissions

Bimodel onset strain relaxation in InAs quantum dots with an InGaAs capping layer

J. F. Chen,[1,a] Ross C. C. Chen,[1] C. H. Chiang,[1] Y. F. Chen,[1] Y. H. Wu,[2] and L. Chang[2]
[1]*Department of Electrophysics, National Chiao Tung University, Hsinchu 30050, Taiwan*
[2]*Department of Materials Science and Engineering, National Chiao Tung University, Hsinchu 30050, Taiwan*

(Received 2 June 2010; accepted 7 August 2010; published online 2 September 2010)

Capping InAs quantum dots (QDs) with an InGaAs layer allows strain relaxation to induce a low-energy electron state below a set of fine dot family states, which is consistent with photoluminescence (PL) spectra. The evolution of InAs thickness suggests a bimodal onset relaxation, i.e., a fine dot family that is strain-relieved by indium outdiffusion from the QDs, as suggested by transmission electron microscopy, and a low-energy dot family that is strain relaxed by the generation of lattice misfits. The indium outdiffusion can explain an abnormal PL blueshift in 70 meV in the fine dot family at onset of strain relaxation. © *2010 American Institute of Physics*. [doi:10.1063/1.3483757]

Understanding the onset of strain relaxation in InAs self-assembled quantum dots (QDs) (Refs. 1–16) is necessary for designing QD devices.[13,14] Strain relaxation in the QDs is accommodated by the generation of threading dislocations in the top GaAs layer and lattice misfits near the front QDs interface,[17] suggesting an occurrence of relaxation toward the top GaAs layer. Growing an InGaAs capping layer on top of the QDs leads to strain relaxation by the generation of the lattice misfits in the bottom GaAs layer near the QDs while the top GaAs layer is dislocation-free.[18] Thus, the InGaAs capping layer can effectively relieve strain in the top GaAs layer and relaxation occurs toward the bottom GaAs layer with an accompanied photoluminescence (PL) blueshift in about 70 meV.[19] This blueshift contradicts an effect of compressive strain reduction in the QDs, which is expected to produce a redshift. This observation suggests a more complicated relaxation than expected. Detailed strain relaxation mechanism has not yet thoroughly established. Therefore, this work describes detailed carrier confinement and PL spectra of the InAs QDs with the InAs deposition thickness over a critical relaxation thickness of 3 ML to understand how the strain is relaxed in the InAs QDs.

The InAs QDs were grown by solid source molecular beam epitaxy. On top of a n^+-GaAs (100) substrate, a 0.3 μm thick Si-doped GaAs ($\sim 7\times 10^{16}$ cm^{-3}) barrier layer, an InAs layer with deposition thickness from 2 to 3.5 ML was deposited at 490 °C (at a rate of 0.26 Å/s) to form the QDs. Following the growth of the QDs layer, a 60 Å $In_{0.15}Ga_{0.85}As$ capping layer and a 0.2 μm thick Si-doped GaAs barrier layer were grown to terminate the growth. The QDs were relaxed by increasing the InAs deposition thickness slightly above 3 ML, as evident from the induction of lattice misfits[18] and a PL blueshift about 70 meV.[19] The QD sheet density was estimated at about 3×10^{10} cm^{-2}. For capacitance-voltage (C-V) profiling, Schottky diodes were realized by evaporating Al with an area of 5×10^{-3} cm^2.

Figure 1 show the simulated and experimental 90 K C-V spectra (at a low-frequency 3 kHz and a high-frequency 100 kHz) and converted experimental electron distribution of a relaxed InAs QDs diode with the InAs deposition thickness of 3.3 ML. Two major C plateaus are visible at the QD layer: a shallow one from −1.5 to −2.2 V, as attributed to a state related to the InGaAs capping layer, and a deep one from

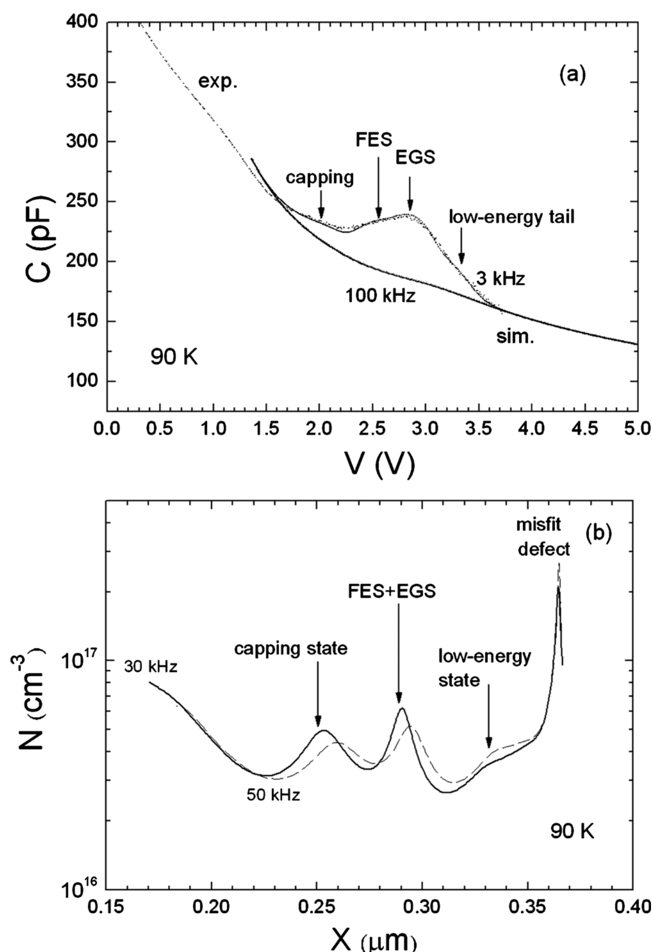

FIG. 1. (a) 90 K experimental and simulated C-V spectra (at a low-frequency of 3 kHz and a high-frequency of 100 kHz) and (b) converted electron distribution of a relaxed InAs QDs diode with the InAs thickness of 3.3 ML. The spectra display a shallow capping-layer state, a fine dot family of the FES and EGS, a low-energy tail and a misfit-related defect state.

a)Electronic mail: jfchen@cc.nctu.edu.tw.

 © 2010 American Institute of Physics

Downloaded 18 Oct 2011 to 140.113.20.108. Redistribution subject to AIP license or copyright; see http://apl.aip.org/about/rights_and_permissions

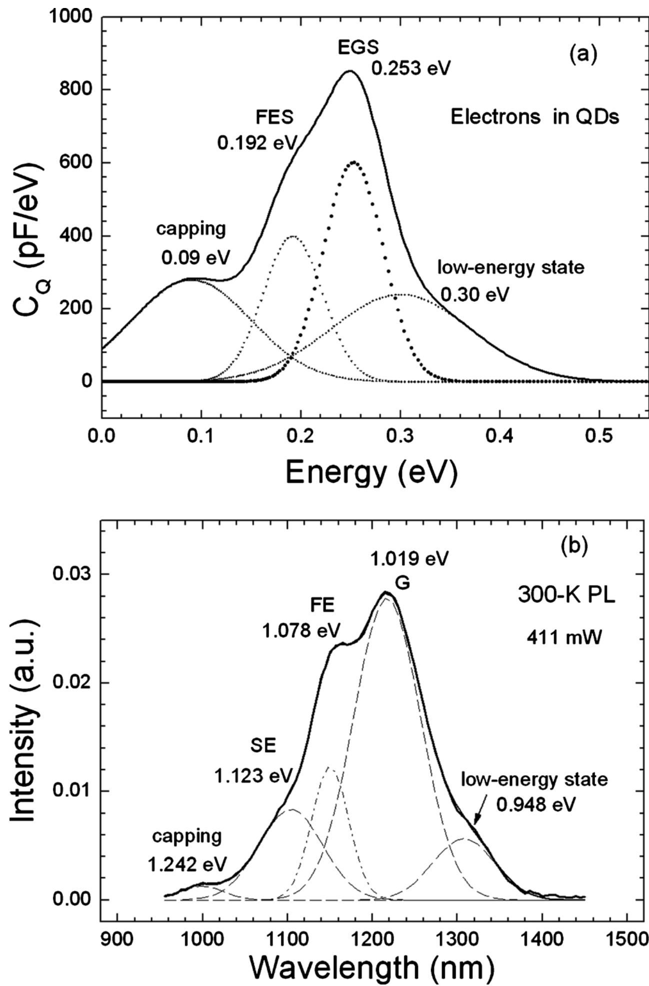

FIG. 2. (a) Gaussian electron distributions of a shallow state, FES, EGS, and a long-tail state used for the simulation in Fig. 1(a). This electron distribution is correlated with the (b) 300 K PL spectra which show a deconvoluted capping-layer emission, the second-excited, first-excited, ground transitions, and a low-energy transition.

−2.2 to −3.5 V, as attributed to a fine dot family consisting of electron ground state (EGS) and first excited state (FES), and an additional low-energy tail. Following these two major plateaus is another carrier confinement related to the misfit-related defect state at 0.35 eV.[18] The experimental carrier distribution in Fig. 1(b) clearly reveals the capping-layer state, the fine dot family, the low-energy tail and the misfit defect state. The carrier confinement is analyzed by a C-V simulation based on a similar treatment,[20,21] where the low-frequency capacitance is expressed by $C_L = dQ_1 + dQ_2/dV = dQ_1/dV + dQ_2/dV = dV_1/dV\boldsymbol{\varepsilon}/L_1 + dQ_2/dV_1 dV_1/dV = (C_1+C_Q)C_2/(C_1+C_Q)+C_2$, where $C_1 = \boldsymbol{\varepsilon}/L_1$ and $C_2 = \boldsymbol{\varepsilon}/L_2$ are the geometric capacitance per unit area across L_1 (distance between the QD layer and the edge of the total depletion width) and L_2 (the depth of the QD layer), and $C_Q = dQ_2/dV_1$ is the occupied density of states of the QDs. The confinement energy E (relative to the GaAs CB edge) of the probed QD electrons can be expressed by $E = V_1 + \boldsymbol{\phi}_n = (q/2\boldsymbol{\varepsilon})N_D' L_1^2 + (kT/q)Ln(N_C/N_D)$, where N_c is the effective density of states in the GaAs CB. Additionally, L_1 is related to the reverse voltage V_R by $V_R = V_1 + V_2 - V_{bi}$, where $V_1 = (q/2\varepsilon)N_D' L_1^2$, $V_2 = (q/\varepsilon)N_D' L_1 L_2 + (q/2\varepsilon)N_D L_2^2 - (L_2/\varepsilon A)\int_{-\infty}^{E} C_Q dE$ and V_{bi} denotes the Schottky barrier height of the GaAs and A is the area of the diode. According to Fig. 1(a), the simulated results (solid curves) correlate well with the experimental data (dotted line) by using Gaussian distributions $C_Q(E)$ of a shallow state peaked at 0.09 eV, a FES at 0.192 eV, a EGS at 0.253, and a long-tail state at 0.30 eV, as shown in Fig. 2(a). Although a better correlation can be achieved, this work neglects the second-excited state to more clearly visualize other contributions. The fitted $E = 0.253$ eV for the EGS and the 50 K PL ground emission at 1.074 eV (1.019 eV at 300 K) give E of a hole ground state (HGS) of $1.50 - 1.074 - 0.253 = 0.173$ eV and a ratio of EGS to HGS of 0.59 to 0.41, a value close to a previously reported 0.61:0.39.[21]

The fitted carrier distribution in Fig. 2(a) has a one-to-one correlation with the deconvoluted PL spectra (at 300 K) in Fig. 2(b), showing a 1.242 eV shallow transition, transitions from a fine dot family including the second excited (SE), first excited (FE), and ground (G) states, and an additional 0.948 eV low-energy transition. The FES and EGS have a similar full-width-half-maximum broadness of about 60 meV as the PL broadness of the FE and ground transitions. According to our results, the 1.242 eV shallow transition displays a significant redshift with an N incorporation into the InGaAs capping layer, and thus is attributed to a

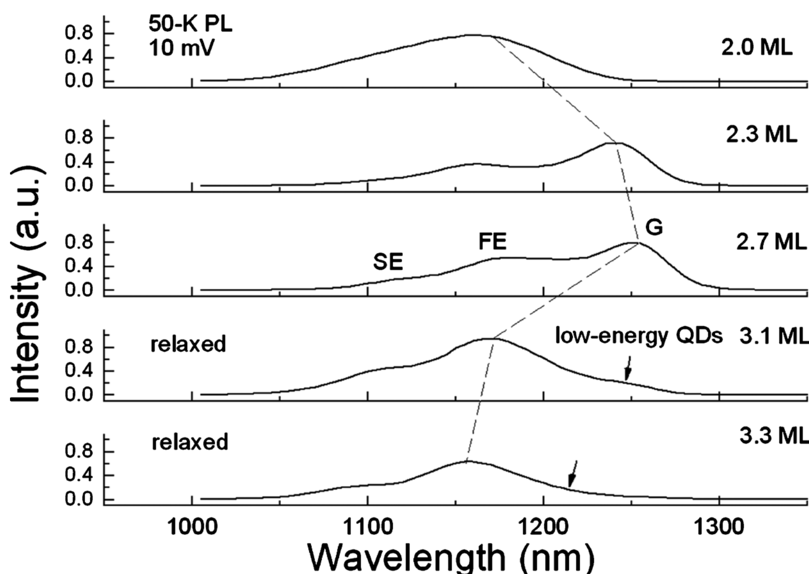

FIG. 3. Evolution of the 50 K PL spectra of the QDs with increasing InAs coverage, under the excitation of 10 mW. For guiding eyes, a dashed line is drawn on the ground transition in the fine dot family. The y-scale is the same for all the spectra.

Downloaded 18 Oct 2011 to 140.113.20.108. Redistribution subject to AIP license or copyright; see http://apl.aip.org/about/rights_and_permissions

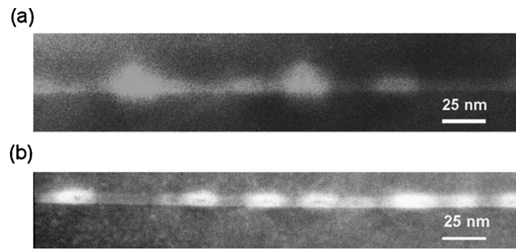

FIG. 4. TEM images of (a) the relaxed 3.1 ML coverage and (b) nonrelaxed 2.7 ML coverage. In the relaxed QDs, bright color emanating out of some QDs can be seen, suggesting indium outdiffusion from the QDs.

state belonging to the capping layer. The above results indicate that onset of strain relaxation does not degrade the feature of the QDs: it displays a fine dot family similar to that observed in nonrelaxed QDs. Onset of strain relaxation mainly induces a low-energy state.

To illustrate the evolution of strain relaxation, Fig. 3 shows the 50 K PL spectra of the InAs QDs with an increasing InAs coverage, under the excitation of 10 mW. A dashed line is drawn to guide the ground emissions from the fine dot family. At the initial formation of the QDs at 2.0 ML, the PL spectra are broad due to large dot-size dispersion at the initial stage. Increasing the InAs coverage increases the dot size and causes a redshift in the ground emission to a maximum of ~1250 nm (~1300 nm at 300 K) at 2.7 ML. The DLTS measurements reveal no defect signals, indicating coherent QD formation. However, when the InAs coverage is increased over a critical thickness of 3 ML to 3.1 ML, the fine dot family still maintains but undergoes an abnormal blueshift in about 70 meV, in addition to the emergence of a low-energy state (at ~1250 nm). When the temperature is lowered (from 300 to 50 K), the low-energy state increases its PL intensity by only a factor of 2, relative to an improvement of a factor of ten in the fine dot family. Because PL can be degraded by defects through which photogenerated carriers are recombined, the low-energy state is ascribed to a degraded dot family due to the misfit defect state at 0.35 eV.[18] This finding suggests a nonuniform strain relaxation: a family of dislocated dots and a fine dot family less affected by misfit defects, as evaluated from its fine, well-resolved emissions that are stronger and sharper than that of the 2 ML nonrelaxed dots.

The blueshift in 70 meV observed in the fine dot family contradicts to the strain relaxation in the QDs because the reduction in a compressive strain in the QDs is expected to increase the lattice constant perpendicular to the growth direction and extend the emission wavelength. Thus, this blueshift cannot be explained by the generation of lattice misfits. The TEM image of the relaxed 3.1 ML coverage, as shown in Fig. 4(a), leads us to attribute the blueshift to indium outdiffusion from the QDs, in which apparent brightness around the tops of some dots and emanated into the top GaAs layer can be seen, in relation to the TEM image of the nonrelaxed 2.7 ML QDs in Fig. 4(b). Previous studies have observed strain related indium segregation.[22,23] This indium outdiffusion can cause a PL blueshift as postgrowth thermal annealing. Thus, the built-in strain in the fine dot family is mainly relieved by the migration of indium adatoms to the top GaAs layer, leading to a reduction in the indium content in the dots and the correlated 70 meV blueshift. According to the results of Fourier transformed TEM images, the dots without the brightness in Fig. 4(a) display significant lattice misfits inside and near the dots. Thus, we attribute these dots to the family of the dislocated dots. A compressive strain reduction in the QDs can produce a low-energy transition. This bimodal relaxation is probably related to the InGaAs capping layer. Without the capping layer, strain relaxation occurs when the QD deposition thickness is increased to 2.8 ML by the generation of threading dislocation in the top GaAs layer and lattice misfits near the QD top boundary, leading to degraded electronic and PL spectra of the QDs without the blueshift.[17]

The authors would like to thank the National Science Council of the Republic of China, Taiwan (Contract No. NSC-97-2112-M-009-014-MY3) and MOE ATU program for financially supporting this research. Dr. J. Y. Chi and R. S. Hsiao are commended for preparing the samples.

[1] F. Heinrichsdorff, M. H. Mao, N. Kirstaedter, A. Krost, and D. Bimberg, Appl. Phys. Lett. **71**, 22 (1997).
[2] D. J. Eaglesham and M. Cerullo, Phys. Rev. Lett. **64**, 1943 (1990).
[3] D. Leonard, K. Pond, and P. M. Petroff, Phys. Rev. B **50**, 11687 (1994).
[4] J. M. Moison, F. Houzay, F. Barthe, and L. Leprince, Appl. Phys. Lett. **64**, 196 (1994).
[5] C. W. Snyder, J. F. Mansfield, and B. G. Orr, Phys. Rev. B **46**, 9551 (1992).
[6] H. Shoji, K. Mukai, N. Ohtsuka, M. Sugawara, T. Uchida, and H. Ishikawa, IEEE Photonics Technol. Lett. **7**, 1385 (1995).
[7] G. Yusa and H. Sakaki, Electron. Lett. **32**, 491 (1996).
[8] J. C. Campbell, D. L. Huffaker, H. Deng, and D. G. Deppe, Electron. Lett. **33**, 1337 (1997).
[9] C. M. A. Kapteyn, F. Heinrichsdorff, O. Stier, R. Heitz, M. Grundmann, and P. Werner, Phys. Rev. B **60**, 14265 (1999).
[10] P. N. Brunkov, A. Patane, A. Levin, L. Eaves, P. C. Main, Y. G. Musikhin, B. V. Volovik, A. E. Zhukov, V. M. Ustinov, and S. G. Konnikov, Phys. Rev. B **65**, 085326 (2002).
[11] W. H. Chang, W. Y. Chen, T. M. Hsu, N. T. Yeh, and J. I. Chyi, Phys. Rev. B **66**, 195337 (2002).
[12] X. Letartre, D. Stievenard, and M. Lanoo, J. Appl. Phys. **69**, 7336 (1991).
[13] H. Drexler, D. Leonard, W. Hansen, J. P. Kotthaus, and P. M. Petroff, Phys. Rev. Lett. **73**, 2252 (1994).
[14] S. Sauvage, P. Boucaud, F. H. Julien, J.-M. Gerard, and J.-Y. Marzin, J. Appl. Phys. **82**, 3396 (1997).
[15] H. L. Wang, F. H. Yang, S. L. Feng, H. J. Zhu, D. Ning, H. Wang, and X. D. Wang, Phys. Rev. **61**, 5530 (2000).
[16] J. F. Chen, R. S. Hsiao, C. K. Wang, J. S. Wang, and J. Y. Chi, J. Appl. Phys. **98**, 013716 (2005).
[17] J. F. Chen, R. S. Hsiao, W. D. Huang, Y. H. Wu, L. Chang, J. S. Wang, and J. Y. Chi, Appl. Phys. Lett. **88**, 233113 (2006).
[18] J. F. Chen, Y. Z. Wang, C. H. Chiang, R. S. Hsiao, Y. H. Wu, L. Chang, J. S. Wang, T. W. Chi, and J. Y. Chi, Nanotechnology **18**, 355401 (2007).
[19] J. F. Chen, R. S. Hsiao, Y. P. Chen, J. S. Wang, and J. Y. Chi, Appl. Phys. Lett. **87**, 141911 (2005).
[20] J. F. Chen, N. C. Chen, J. S. Wang, and Y. F. Chen, IEEE Trans. Electron Devices **48**, 204 (2001).
[21] S. D. Lin, V. V. Ilchenko, V. V. Marin, K. Y. Panarian, A. A. Buyanin, and O. V. Tretyak, Appl. Phys. Lett. **93**, 103103 (2008).
[22] M. O. Lipinski, H. Schuler, O. G. Schmidt, K. Eberl, and N. Y. Jin-Phillipp, Appl. Phys. Lett. **77**, 1789 (2000).
[23] J. G. Garcı´a, J. P. Silveira, and F. Briones, Appl. Phys. Lett. **77**, 409 (2000).

Downloaded 18 Oct 2011 to 140.113.20.108. Redistribution subject to AIP license or copyright; see http://apl.aip.org/about/rights_and_permissions